PASSIVE DC-DC CONVERSION TECHNIQUE FOR VIBRATION ENVIRONMENTS AND ITS APPLICATION IN RFID SYSTEMS

by

SREE KALYAN RAVILLA

B.Tech in Electronics and Communication Engineering, Jawaharlal Nehru Technological University, India, 2006

Submitted to the Graduate Faculty of

Swanson School of Engineering in partial fulfillment

of the requirements for the degree of

Master of Science

University of Pittsburgh

2010

UNIVERSITY OF PITTSBURGH

SWANSON SCHOOL OF ENGINEERING

This thesis was presented

by

Sree Kalyan Ravilla

It was defended on

April 2nd, 2010

and approved by

William E Stanchina, Professor, Electrical and Computer Engineering Dept.

Ronald G Hoelzeman, Associate Professor, Electrical and Computer Engineering Dept.

Thesis Advisor: Marlin H Mickle, Professor, Electrical and Computer Engineering Dept.

PASSIVE DC-DC CONVERSION TECHNIQUE FOR VIBRATION ENVIRONMENTS AND ITS APPLICATION IN RFID SYSTEMS

Sree Kalyan Ravilla, M.S

University of Pittsburgh, 2010

DC-DC conversion circuits are implemented in several electronic devices to achieve higher power densities. The switched mode DC-DC converters are known for their higher power conversion efficiencies and can transform the energy stored in the passive elements to higher voltage levels than the input voltage (boost converter) or even to lower voltage levels (buck converter) than the input voltage. All the switched mode DC-DC converters use active elements to produce the switching action which consume reasonable amount of power. Hence, the overall power requirement of the device is increased and this would be very critical for low power applications. The active elements can be replaced by passive electromechanical switches which produce electrical switching action by utilizing the energy from the ambient sources. The research work focuses on utilizing the vibrations present in the environment to produce the electrical switching action in passive elements. The new technique proposed adopts the passive motion activated electro-mechanical switch, with a ball bearing making intermittent contacts between the inner conductor and the outer conductor. A conducting path is established when the ball bearing comes in contact with the inner conductor and the outer conductor simultaneously.

The passive DC-DC conversion technique is further analyzed by discussing its application in RFID systems which operate on very low power constraints. The improvement in the output voltage levels is proved by comparing the output DC voltage levels generated from

the radio frequency signal by employing the DC-DC conversion technique with the voltages obtained without the DC-DC conversion technique.

TABLE OF CONTENTS

LIST OF TABLES

LIST OF FIGURES

PREFACE

I would like to express my sincere gratitude to Dr. Marlin Mickle, Department of Electrical and Computer Engineering, for making this work possible. I highly appreciate his efforts in advising me and the support provided for completion of my graduation. I am thankful to him for accepting me into RFID research group and suggesting this topic for my thesis.

I would also like to convey my special thanks to Dr. Peter Hawrylak and Dr. Ajay Ogirala for providing continuous support in filling gaps in my work. I would like to mention the help provided by people in Sound Systems and structures lab by lending their equipment for the current thesis work. I would like to thank Dr. William E. Stanchina and Dr. Ronald G. Hoelzman for accepting my invitation to be a part of my thesis committee.

1.0 INTRODUCTION

The passive electro-mechanical switch, which produces switching action due to vibrations or motion in the switch, provides huge benefits for low power applications by substituting the functionalities of an active transistor switch in certain environments subject to motion. The switch can be used to transform a low DC voltage to a high DC voltage using different DC-DC conversion circuit topologies which are discussed later in this work. The passive conversion technique is of particular interest and can be utilized in the field of low power applications where the operation of the devices is strictly limited by the power constraints. RFID systems are one of those low power applications where the tags run on the power harvested from the reader transmission or internal power supply from on-board batteries. The low voltage level generated by the tag can be transformed to a higher DC voltage to power the data processing logic embedded in the tag and also the range of tag can be increased by producing higher voltage levels for a given field strength.

1.1 MOTIVATION AND CONTEXT

The increasing demand of low power applications and proliferation of remotely powered devices resulted in continuous growth in demand for devices that operate at voltage levels below 1.2 V and a very low load current (< 1uA) [1][2]. In most of the applications, though the power

requirement is achieved, sufficient voltage levels are not produced to power the circuitry. In addition to that, the voltage requirements will vary for different sections in the circuit. For example, the digital section of the circuit can work at very low voltage levels but the analog section requires high voltage levels. Multiple voltage sources cannot be placed to produce the required voltage levels and at the same time a simple voltage divider circuit with resistors can produce lower voltages but are very inefficient. The DC-DC converters offer many advantages by eliminating the requirement of multiple voltage sources and at the same time producing the desired voltage levels at very high efficiency. The DC-DC converters can generate higher voltage level or a lower voltage level depending upon the requirement and also invert the polarity of input voltage. Though there are many DC-DC conversion techniques proposed in literature for low power applications, most of the techniques utilize active transistor elements which suffer from the disadvantage of power overhead as these active elements require power to drive the gate-to-source voltages. Though the power consumed by the active elements would not be critical when the applications work at higher power levels, it would be a limiting factor for low power applications. Hence, the active transistor elements need to be replaced by a passive element to avoid the power overhead. The motion activated electro-mechanical switches which utilize the vibrations in the environment to produce the desired switching action are a viable option to replace the active transistor switches.

One of the benefits of the proposed passive DC-DC conversion technique is in the field of RFID systems where sufficient power levels are harvested by the tags but higher voltage levels need to be obtained to power the logic circuitry at the same energy levels. Hence, the passive DC-DC conversion yields higher voltages with high power conversion efficiencies and eliminates the need of power consuming active elements. Figure 1 shows the block diagram

description of the passive RFID tag circuitry where the DC-DC conversion can be implemented to boost the voltage levels required for the operation of the logic circuitry. The frequency of the energy field is normally too high to allow a DC-DC converter to be used to achieve higher voltages. The rectification circuit followed by the switch action essentially provides a “frequency downshifting” to take advantage of DC-DC conversion.

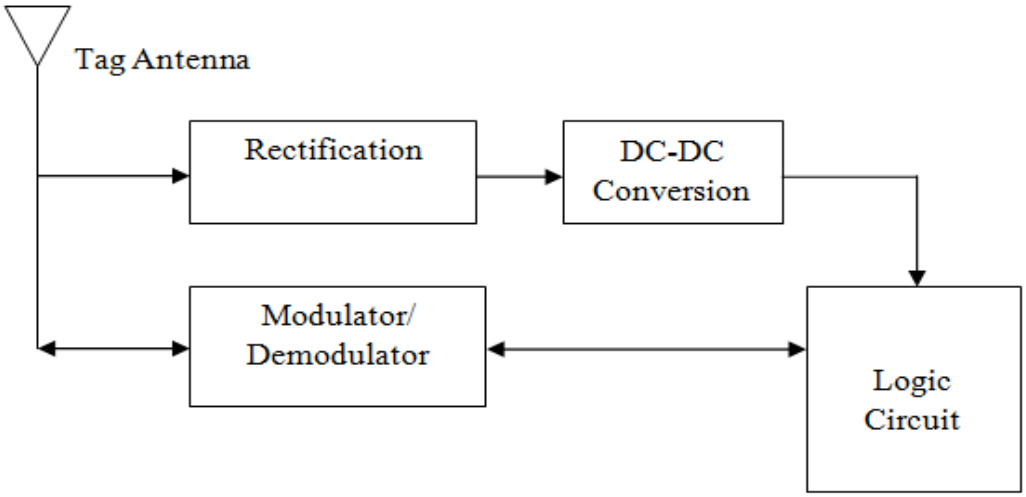

Figure 1. Tag Circuit Block Diagram

The motion-activated passive DC-DC conversion technique is best suited to environments like surface of ocean, moving vehicles, human body, etc., which can essentially induce constant motion in a ball bearing inside the electro-mechanical switch which provides the switching action. Several switches can be placed in parallel or series configurations to obtain high frequency switching action and even the dimensions of the switch can be varied to increase or decrease the frequency of switching, which is discussed in this thesis.

1.2 STATEMENT OF THE PROBLEM

The initial focus of this work is to prove the feasibility of implementing a passive DC-DC conversion circuit that adopts the motion activated electro-mechanical switch, which produces switching action when subjected to vibrations. The switching characteristics of the electro-mechanical switch need to be analyzed by varying the intensity of vibrations. Based on the intensity and frequency of vibrations and the physical dimensions of the switch, the dynamics of ball bearing inside the switch need to be investigated. For given vibration characteristics of the environment, the approach to tune the design of the switch to exhibit efficient switching phenomena needs to be analyzed. The implementation of the switch to generate higher voltages than the input voltage in different DC-DC conversion circuit topologies should be verified by replacing the active elements in the circuits with the motion activated switches. The pros and cons of different configurations will be studied. The feasibility of implementing micro-switches for on-chip DC-DC conversions will be discussed and a step towards implementing printed inductor transformers is analyzed in order to reduce the size of components on board.

The remainder of the research is focused on applying the proposed technique in the RFID systems. The radio frequency signal will be fed to the rectification circuit which converts the RF signal into DC signal and the DC voltage obtained after rectification will be boosted to a higher voltage by implementing the proposed technique.

1.3 GOALS OF RESEARCH

- ✓ Demonstrate the ability to amplify low DC input voltage to a sufficient voltage to switch transistors.
- ✓ Investigate the properties of motion-activated switch to harvest the vibration energy and discuss the parameters of the switch to tune the design of switch to perform efficiently at a given intensity of vibration.
- ✓ Evaluate traditional DC-DC topologies and demonstrate at least one promising topology to implement the motion-activated switch.
- ✓ Integrate all facets of the DC amplification into a working proto-type system.
- ✓ Incorporate air core printed PCB transformers to obtain the necessary AC amplification.

2.0 BACKGROUND ON RFID SYSTEMS

Radio Frequency Identification (RFID) technology is a challenging field which enables wireless identification from a distance. RFID technology steadily replaced the earlier bar-code technology where unlike bar-code, RFID does not require line of sight for identification. The RFID systems primarily consist of readers and a set of tags attached to the objects to be identified. The reader initiates the communication with tags and each of the tags responds to the reader's query for self-identification. There are several ways to classify RFID devices. Mainly, RFID devices are classified into active and passive devices. The active devices need an internal power supply for operation which increases the maintenance cost of the overall system. On the other hand, the passive devices operate on the power harvested from the reader's transmission thereby reducing the maintenance cost of the overall system by providing indefinite lifetime of operation. The most important frequency ranges for RFID systems are 0-135 kHz (North and South America and Japan (0- 400 kHz)), ISM frequencies around 6.78 MHz, 13.56 MHz, 27.125 MHz, 40.68 MHz, 433.92 MHz, 869 MHz, 915 MHz, 2.45 GHz, 5.8 GHz and 24.125 GHz [3]. In the case of passive tags, the transfer of power between the reader and the passive tag is accomplished either by inductive coupling or electromagnetic propagation. RFID systems that transfer power by inductive coupling operate in the near field of the antenna. The reader passes a large alternating current through the reader coil which generates a magnetic field in the near-field of the antenna. The magnetic field created by the reader induces current in the tag's antenna coil and the tag

transmits the data back by load modulation. The inductive coupling is widely adopted in passive RFID systems and hence resulted in standards, ISO 15693 and 14443. The RFID devices operating in the far field capture the RF signal from reader and communicate back by using the back scattering technique in which the tag's antenna impedance is changed to vary the reflection of the incoming signal due to mismatch.

2.1 ANTENNAS

Antenna serves the purpose of transmitting and receiving the radio frequency signal between the reader and the tag. The antennas are fundamentally characterized by properties like radiation pattern, directivity, gain, impedance and polarization. The antenna's radiation pattern is defined as the graphical representation of radiation properties as a function of space coordinates. Radiation properties include power density, field strength and gain. The gain of the antenna is defined as the ratio of radiation intensity in a given direction to the radiation intensity from an ideal isotropic antenna for the same input power levels. The gain of an antenna is normally measured in dBi (decibels referenced to an isotropic antenna). The directivity of the antenna defines the directional properties of the antenna. The antenna offers large range, if the maximum directivity is in the direction of the incoming wave. Polarization is defined as the orientation of the electric field of the electromagnetic wave. Polarization is typically classified as linear and circular. The electric field lies in one plane for linear polarization and in circular polarization the electric field rotates about the direction of propagation of the electromagnetic wave. If the polarization of the receiving antenna is not in the same direction as the incoming wave, then there is reduction in the received power because of the polarization loss.

The input impedance of the antenna is defined as the ratio of voltage to current at any given point or the ratio of appropriate components of electric to magnetic field at a given point. From the maximum power transfer theorem, the input impedance of the antenna should be matched to the load impedance of the receiving antenna to transfer maximum power. In the case of transmitting antenna the source impedance should be matched to the input impedance of the antenna to allow maximum transfer of power.

For the receiving antenna connected to a load shown in Figure 2-(a), the ratio of the voltage to current at the terminal A-B with no load connected defines the input impedance of the antenna.

$$Z_A = R_A + j\,X_A \tag{2.1}$$

Where R_A is antenna resistance and X_A is the antenna reactance. The resistive part consists of two components

$$R_A = R_r + R_L \tag{2.2}$$

Where R_r is Radiation resistance and R_L is the loss resistance of the antenna

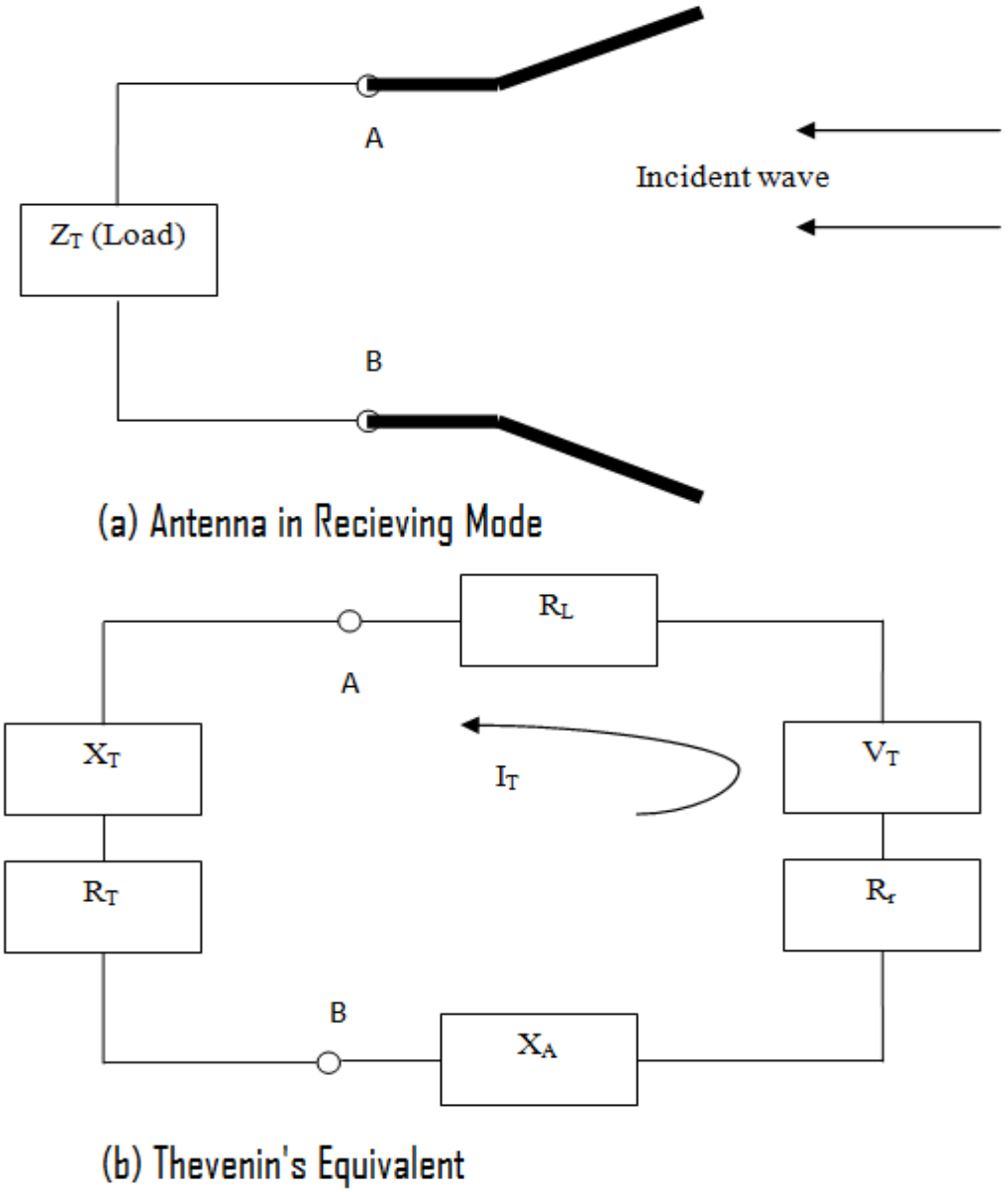

Figure 2. Receiving Antenna Equivalent Circuit

In the Thevenin's equivalent circuit [4], V_T is the voltage induced and R_T and X_T are the resistance and reactance of the load. It can be easily shown that the power delivered to Z_T is

maximized when the load impedance is complex conjugate of the antenna impedance [4]. That is when

$$R_T = R_A = R_r + R_L \tag{2.3}$$

$$X_T = - X_A \tag{2.4}$$

If the antenna impedance is mismatched with the load, then voltage reflection occurs which is usually represented by the voltage reflection coefficient Γ.

$$\Gamma = \frac{Z_T - Z_A}{Z_T + Z_A} \tag{2.5}$$

In addition to the impedance mismatch, the bandwidth of the antenna causes severe impedance mismatch for frequencies outside the frequency range. Bandwidth of the antenna is defined as the range of frequencies within which the performance of the antenna, with respect to some characteristic, conforms to specified standard.

2.2 FRIIS EQUATION FOR FAR-FIELD TRANSMISSIONS

The Friis equation relates the power received to the power transmitted between the two antennas separated by a distance $R > 2D^2/\lambda$, where D is the largest dimension of transmitting or receiving antenna and R defines the boundary between the near field and the far field. The Friis equation can be used to calculate the received power at the tag's antenna in far field. The Friis equation is given by

$$P_r = P_t\, G_t(\theta_t, \Phi_t)\, G_r(\theta_r, \Phi_r)\, (1-|\Gamma_t|^2)\, (1-|\Gamma_r|^2)\, (\lambda/4\pi R)^2 |\rho_t * \rho_r|^2 \tag{2.6}$$

P_r is the power received, P_t is the power transmitted, $G_t(\theta_t, \Phi_t)$ and $G_r(\theta_r, \Phi_r)$ are the gain of the transmitting and receiving antennas, $(1-|\Gamma_t|^2)$ and $(1-|\Gamma_r|^2)$ are the loss factors due to impedance mismatch at the transmission and the receiver end. $(\lambda/4\pi R)^2$ is the free space loss factor and $|\rho_t * \rho_r|^2$ is the polarization loss. Figure 3 shows the coordinates system for analysis

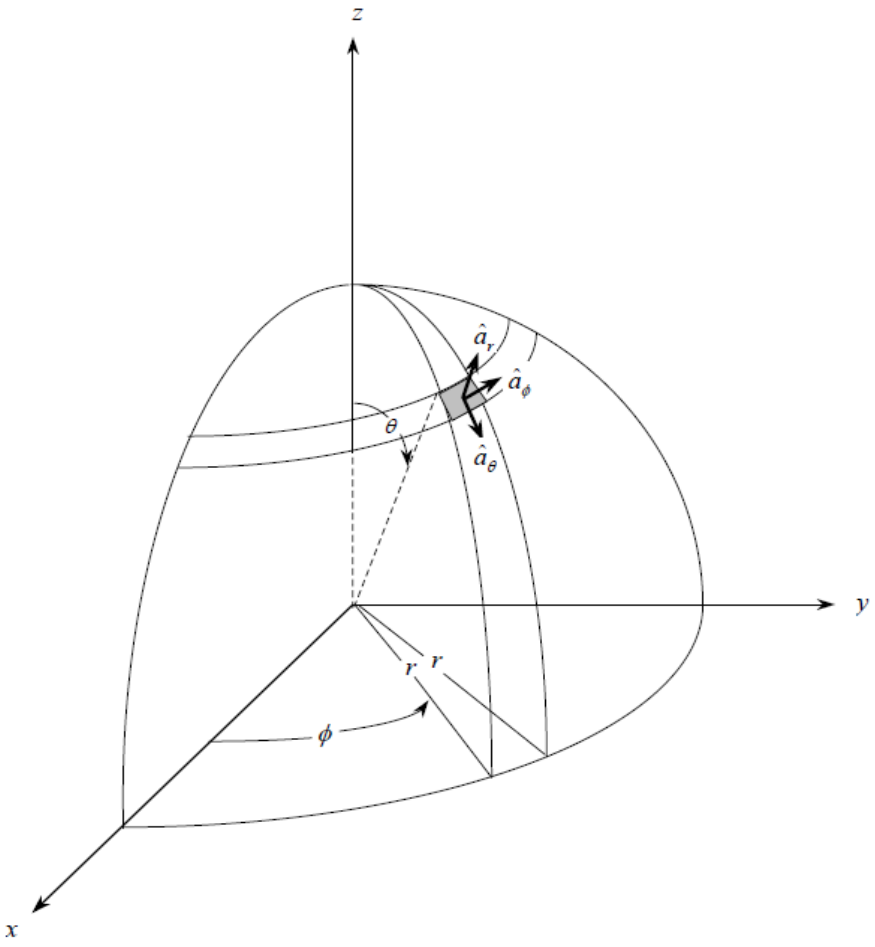

Figure 3. Coordinate system for antenna analysis

3.0 MOTION ACTIVATED ELECTRO-MECHANICAL SWITCH

The motion activated electro-mechanical switch [5] consists of a ball bearing, a conducting circular washer and other conducting traces. The ball bearing is made to move between the inner and outer conductors where the inner and outer conductors are electrically isolated. The ball bearing moves over the flat circular copper trace which is the inner conductor, and the movement is confined by a circular washer which is the outer conductor. Figure 4 indicates the motion-activated switch.

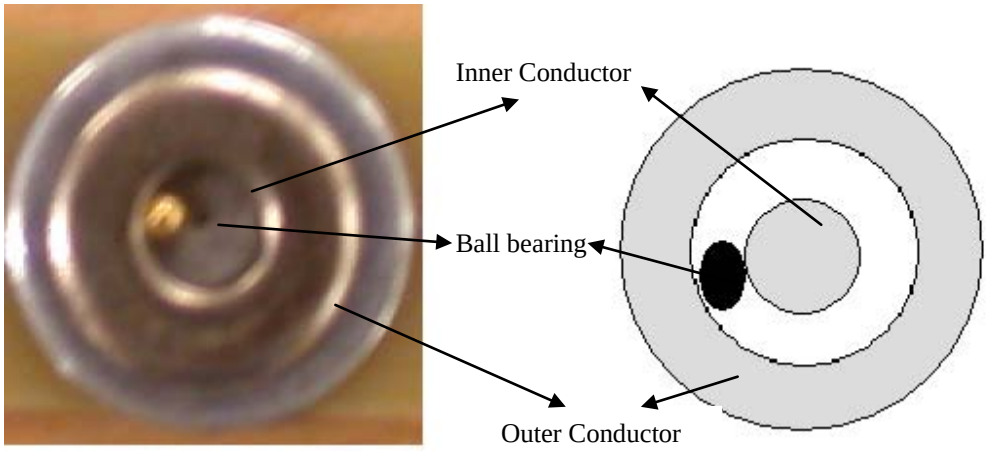

Figure 4. Motion-activated switch

An electrical connection is established between the inner conductor and the outer conductor when the ball bearing makes contact with the washer. When the switch is subjected to vibrations,

the ball bearing is confined to move inside the washer making intermittent contact between the inner and outer conductors. When the ball bearing makes contact with both the inner and outer conductors, the switch is in closed state. Figure 5 shows the motion activated electro-mechanical switch implementation in a circuit and its electrical equivalent is given in Figure 6.

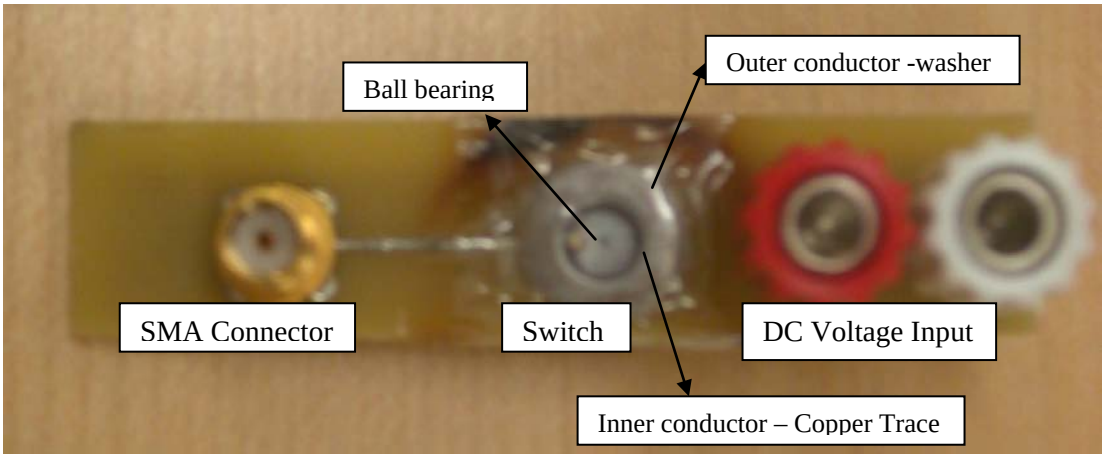

Figure 5. Motion activated electro-mechanical switch implementation

A DC voltage of 3 volts is applied to the terminals a and b as indicated in the electrical equivalent circuit in Figure 6, and the output from the SMA connector is observed from the terminal c and d as shown in Figure 6. The switching characteristics exhibited by the switch are shown in the Figure 7.

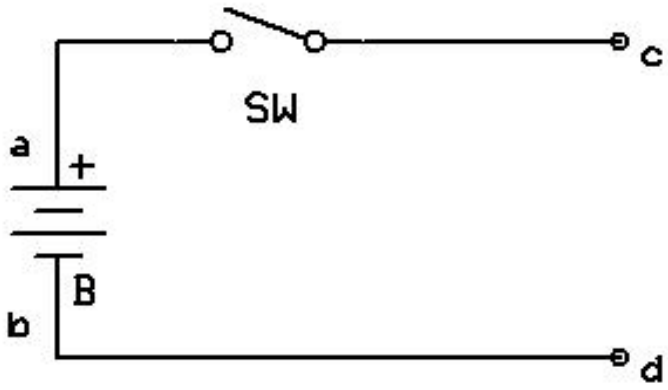

Figure 6. Electrical equivalent of motion activated switch

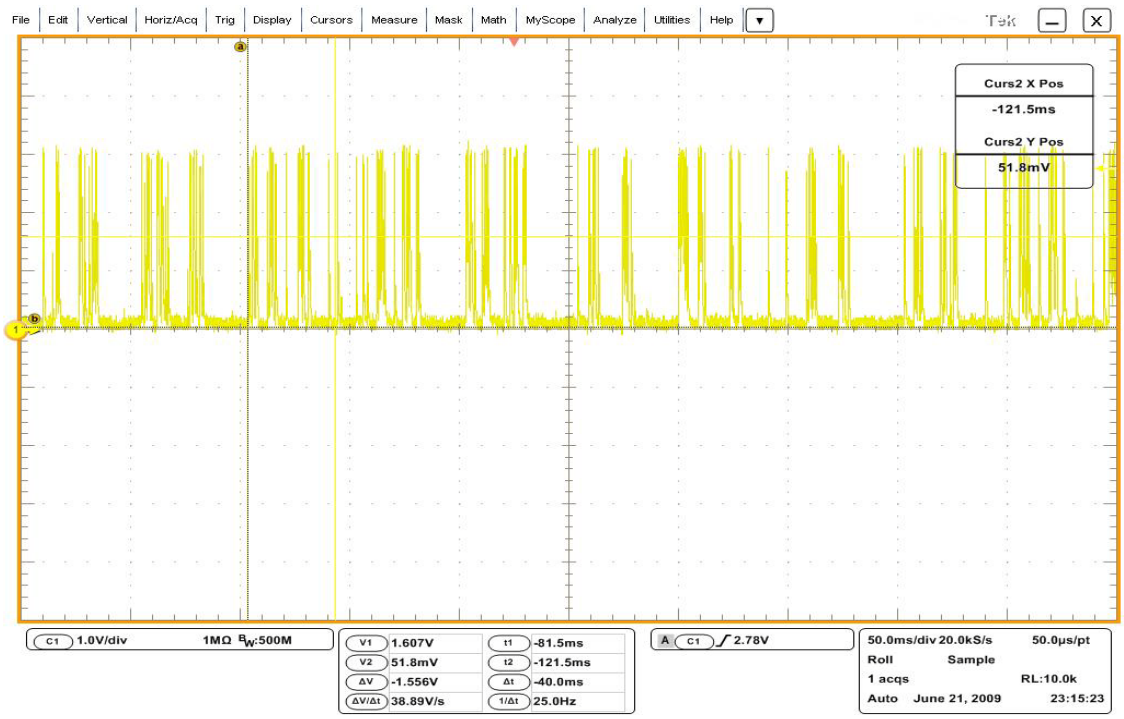

Figure 7. Switching characteristics exhibited by the switch

3.1 IMPLEMENTATION OF SWITCH

The motion activated electro-mechanical Switch foot print demonstration prototype is designed on a 2-layer PCB using the expressPCB software. The footprint consists of an inner conductor which is a round pad via with diameter 0.16 inches and with hole size of 0.020 inches and a ring shaped outer conductor which is an arc with radius of 0.153 inches and line width of 0.100 inches. The inner conductor and the outer conductor are electrically isolated, and the inner conductor connects to rest of the circuitry through a via. Figure 8 shows the foot print of the switch.

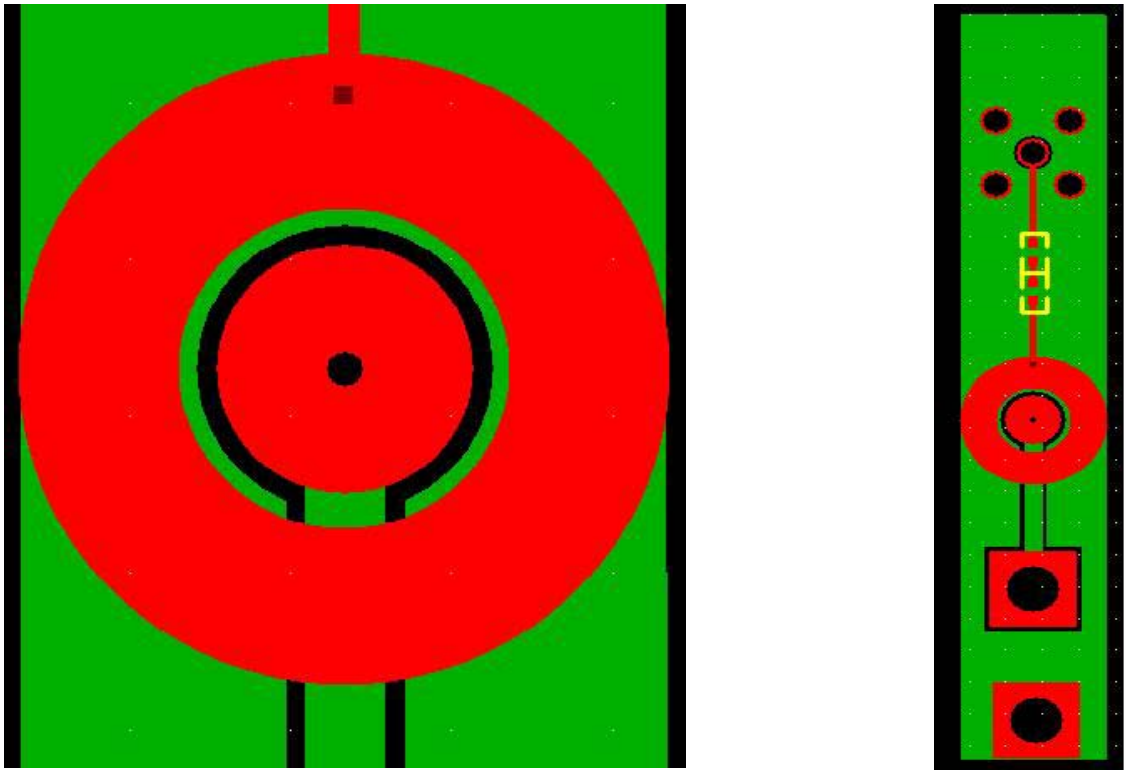

Figure 8. PCB foot print of motion activated switch

The conducting circular washer is placed on the outer trace, and a conducting ball bearing is allowed to move inside the washer. The top surface of the washer is closed with a transparent material to contain the ball bearing. The transparent material facilitates in observing the dynamics of the ball bearing inside the washer.

As the ball bearing attains higher velocities, there might be risk of the bearing lifting above the surface and hence, an electrical contact is never established with the inner conductor. The washer should be designed in such a way that the ball bearing should make contact with the bottom surface all the time and at the same time the movement of the ball bearing is not obstructed. It is observed that by placing two washers of different sizes with reduced thickness, one above the other as shown in the Figure 9 and Figure 10, will perform more efficiently than placing a single washer. By placing two different washers one over the other also offers the advantage of varying the diameter of the top washer to further investigate the switching action based on the physical dimensions of the washer.

Figure 9. Two washers of different sizes

Figure 10. Two washers of different sizes stacked one over the other

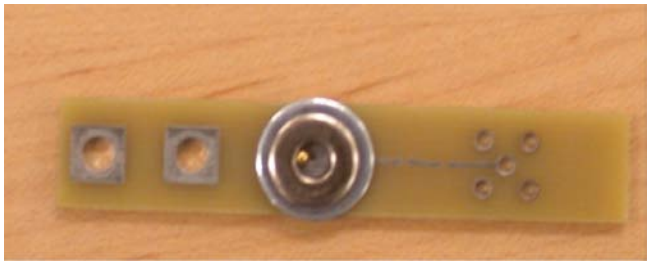

Figure 11. Electro-mechanical switch with washers placed one over the other

The two different setups for placing the washer are verified by analyzing the free body diagrams of the all forces acting on the ball bearing in the two different setups. Figure 12 shows the two different setups.

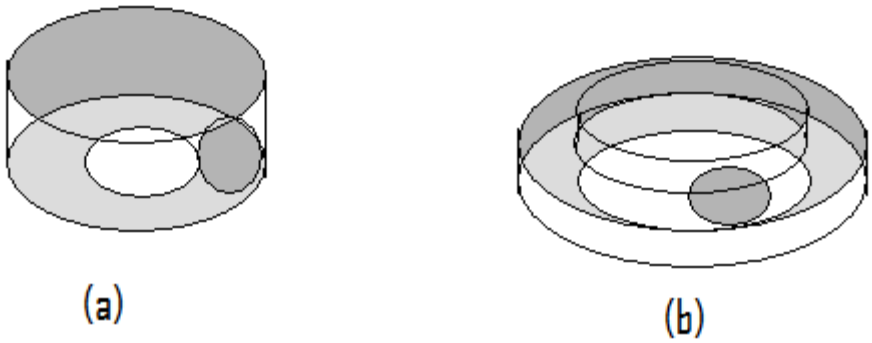

Figure 12. (a) Setup 1 - Single washer (b) Setup 2 - Two washers placed one over the other

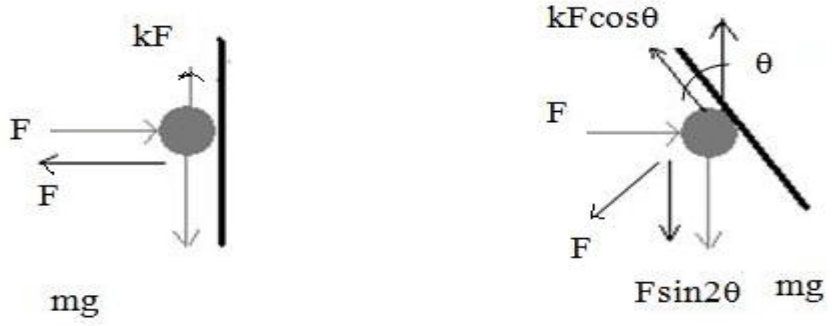

Figure 13. Free body diagrams (a) Setup 1 (b) Setup 2

Figure 13 shows the free body diagrams of all the forces acting on the ball bearing for the two different setups. The force F is the centripetal force acting on the ball bearing when the bearing attains sufficient velocity. The centripetal force is given by

$$F = \frac{mV^2}{R} \tag{3.1}$$

where m is the mass of the ball bearing, V is the velocity attained by the ball bearing and R is radius of the washer.

The gravitational force acting on the washer is given by ‘mg’, where g is the gravitational constant (g =9.8 m/sec^2). The frictional force is given by kF, where k is the frictional constant and F is the centripetal force acting on the ball bearing.

The net force acting on the ball bearing downwards for setup 1 is given by

$$\text{Force downward} = mg - kF \tag{3.2}$$

The net force acting on the ball bearing downwards for setup 2 is given by

$$\text{Force downward} = mg + F\sin 2\theta - kF\cos^2\theta \tag{3.3}$$

Hence, the net force acting downwards for the setup 2 is greater than the net force acting downward for the setup 1. In setup 2, the chances for lifting above the bottom surface is less compared to setup 1.

3.2 FREQUENCY RESPONSE OF SWITCH

The frequency of switching for different vibration intensities is analyzed using the spectrum analyzer. The highest frequency peak corresponds to the fundamental switching frequency

component for the given intensity of vibration. For different vibration characteristics, the switch exhibited different fundamental switching frequencies. The switch is subjected to vibrations using the equipment as shown in Figure 14. Figure 14-(a) provides a platform that rotates circularly and Figure 14-(b) provides a platform that vibrates linearly.

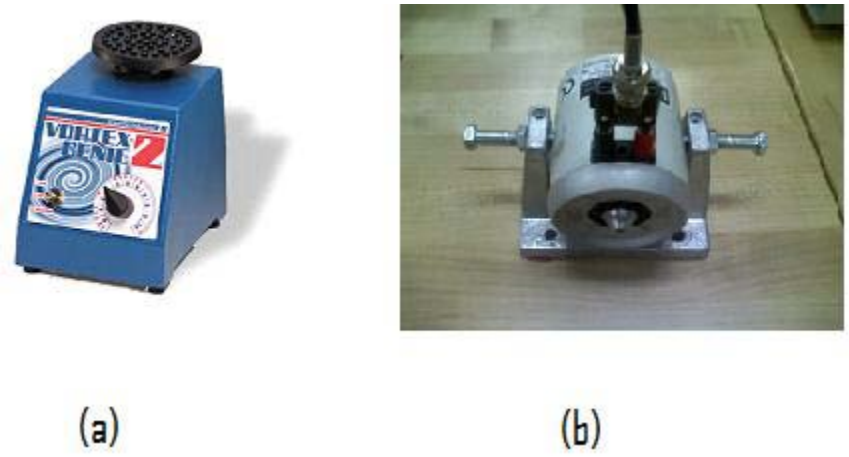

Figure 14. Vibration Platforms (a) Circular Motion (b) Linear Motion

3.2.1 Circular Motion

The vortex genie-2 laboratory equipment is used to cause circular motion in the switch. The switch is subjected to different angular velocities (RPM) to analyze the switching frequencies. The angular velocity is varied from 600 RPM to 3600 RPM and the peak switching frequency for the respective angular velocity is observed on the spectrum analyzer. Table 1 illustrates the peak switching frequency observed on the spectrum analyzer for different revolutions per minute (RPM). The plot for the peak switching frequency versus the input motion is shown in Figure 15.

Table 1. Peak switching frequencies for circular motion

Sl No	Approx. RPM	Approx. Freq (Hz)	Switch Peak Frequency (Hz)
1	600	10	10.125
2	900	15	11.25
3	1200	20	14.125
4	1500	25	16.75
5	1800	30	18.25
6	2100	35	22
7	2400	40	24.125
8	2700	45	26.25
9	3000	50	30.625
10	3300	55	38.875
11	3600	60	No Peak Found

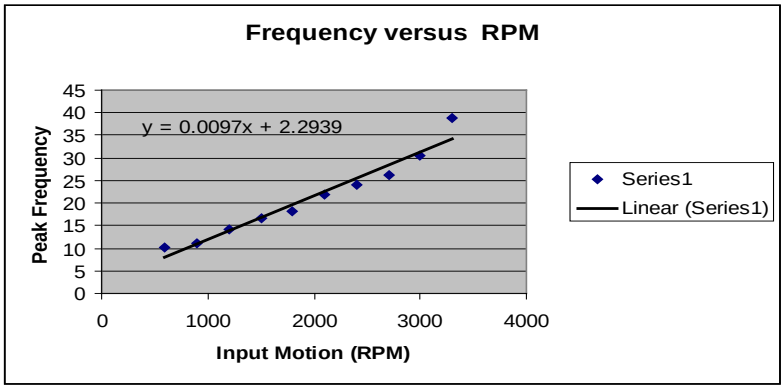

Figure 15. Plot of Peak Switching frequency vs. input motion

From Figure 15, the relationship is considered linear based on relative precision of data points. Figure 16, illustrates the spike generated when a contact is established. The switching period (T) between two successive peaks can be approximated by estimating the dynamics of the ball bearing inside the washer.

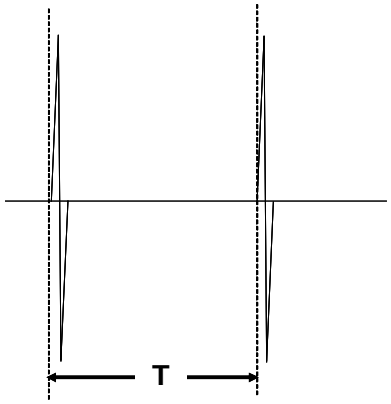

Figure 16. Switching period T between two successive contacts

Consider as one example, the peak switching frequency of 14.125 Hz listed in the Table 1. Based on this frequency, 1/T, is 1/14.125 or 0.07079 seconds. At Setting 3, the RPM is 1,200 RPM. Thus, from one point of motion, the time to return to the same point is

(1,200 Revolutions/Minute)*(Minute/60 Seconds) = 20 Revolutions/Second (3.4)

Thus, there should be two contacts by the spherical conductor per revolution (one on each side) giving a time between contacts of 0.1 Seconds. However, the time between contacts as per the output frequency is 0.07079 Seconds, which is considerably shorter than the 0.1 Seconds

from the rotational velocity motion input to the system. The rotational motion thus provides both X and Y velocity components as shown in Figure 17. It is assumed the X and Y components are equal. Note that by the Pythagorean Theorem applied to the two sides of the square and the diagonal of Figure 17.

$$\{(0.7079)^2 + (0.0709)^2\}^{1/2} = 0.1 \text{ seconds} \quad (3.5)$$

Therefore, the actual motion pattern of the spherical conductor is as shown by the center lines forming the square inside the circle of Figure 17. Thus, the period, T, of Figure 16, is given by:

$$(2^{1/2}/2)*14.125 = 9.9879 \approx 10 \text{ Hz} \quad (3.6)$$

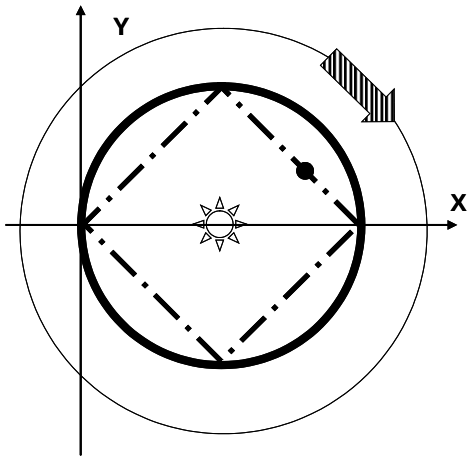

Figure 17. Dynamics of the ball bearing

The primary dynamics of the spherical conductor bounding inside the outer conductor are determined by the mass of the spherical conductor and the size of the cavity within the outer conductor and gravity. The path indicated in Figure 17, continues through the increases in RPM until the RPM reaches 3000. At that point, the velocities in the X and Y dimensions are such

that the spherical conductor simply has no stable pattern giving contacts that simply are approaching a random pattern. Hence, the linear range shown in Figure 15 provides the predictable region of operation of the switch.

3.2.2 Linear Motion

The linear electro-dynamic shaker shown in Figure 14 (b) is used for rest of the work. The experimental setup for measuring the frequency response is shown in Figure 18. The experimental setup utilizes an electro-dynamic linear shaker which is used as a platform to produce a linear vibration environment. The shaker's platform is displaced linearly in one plane and the displacement is proportional to the amplitude of the sinusoidal waveform applied from the function generator. Hence, for one cycle of sinusoidal waveform, the shaker's platform is displaced to maximum in forward direction and moves in the reverse direction till the maximum distance crossing the original position and then returns to the original position.

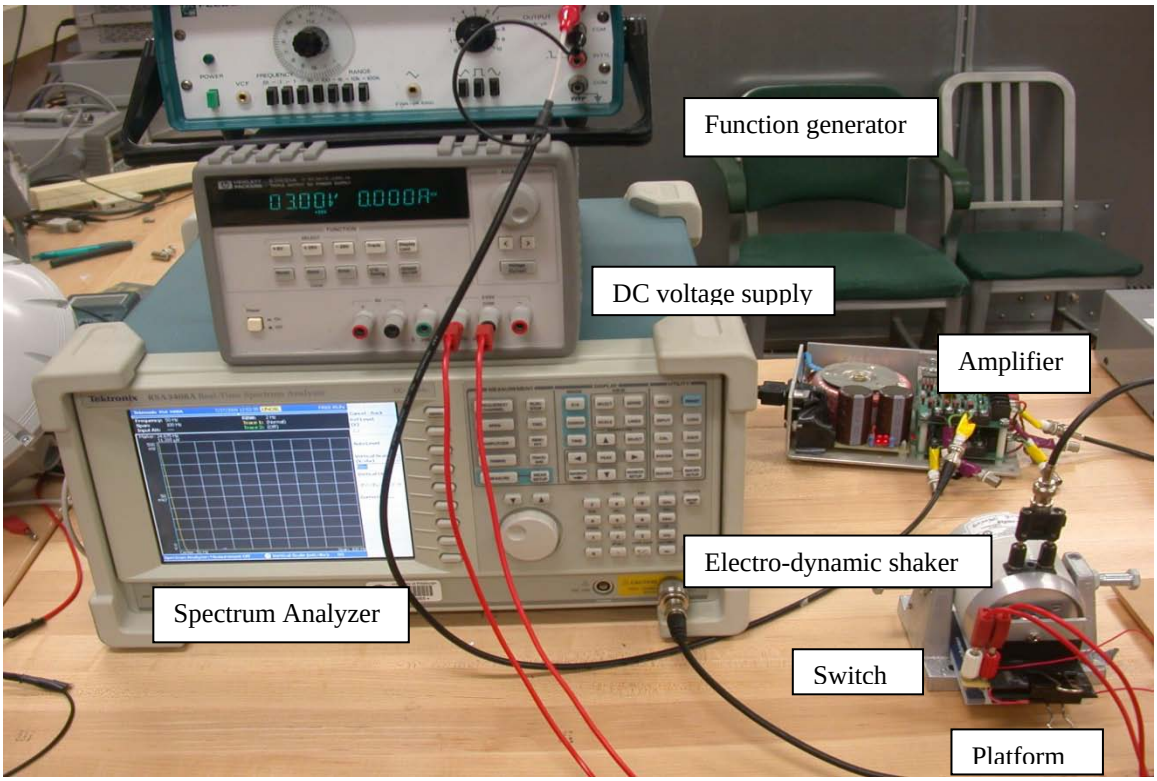

Figure 18. Experimental setup to measure the frequency response of switch

The vibration intensity of the shaker is varied by changing the frequency of a sine wave from the function generator serving as the shaker modulation. The amplifier provides the required voltage level for the electro-dynamic shaker. The switch is connected to 3 volts DC voltage source, and the switch is made to vibrate using the electro-dynamic shaker as shown in the experimental setup. The output from the switch is observed on the spectrum analyzer. The frequency of vibration of the shaker is varied from 10 Hz to 50 Hz in the function generator. Figure 19 to Figure 23 show the frequency response obtained from the spectrum analyzer.

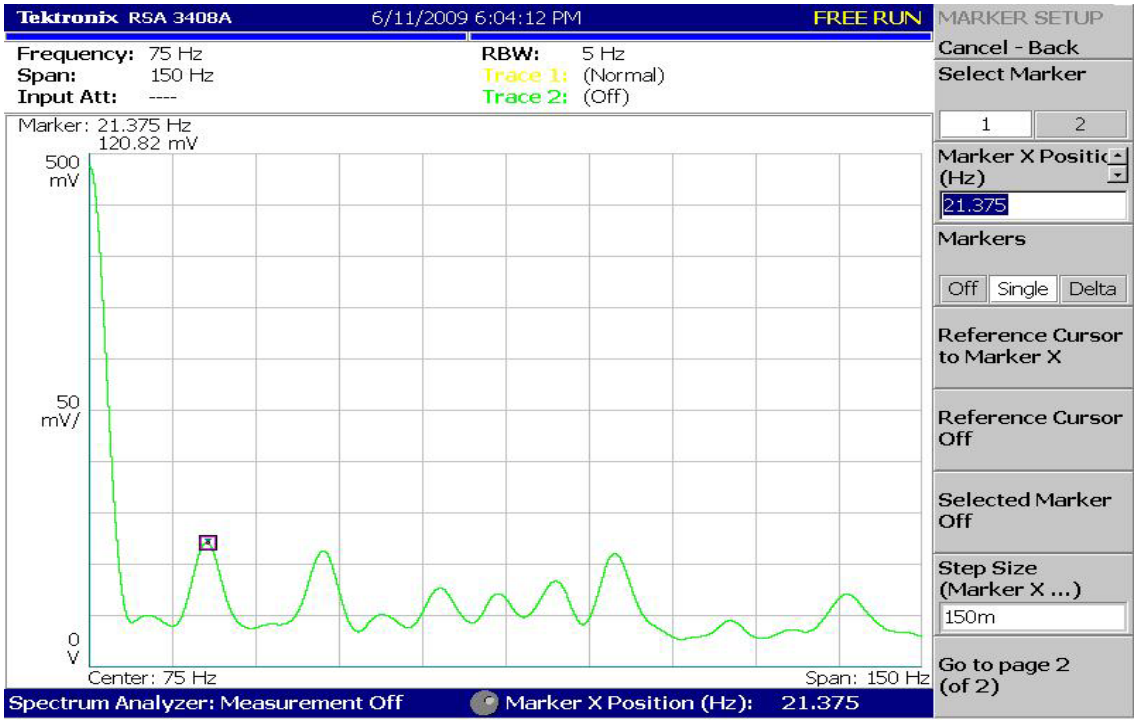

Figure 19. Frequency response for 10 Hz input frequency to the shaker

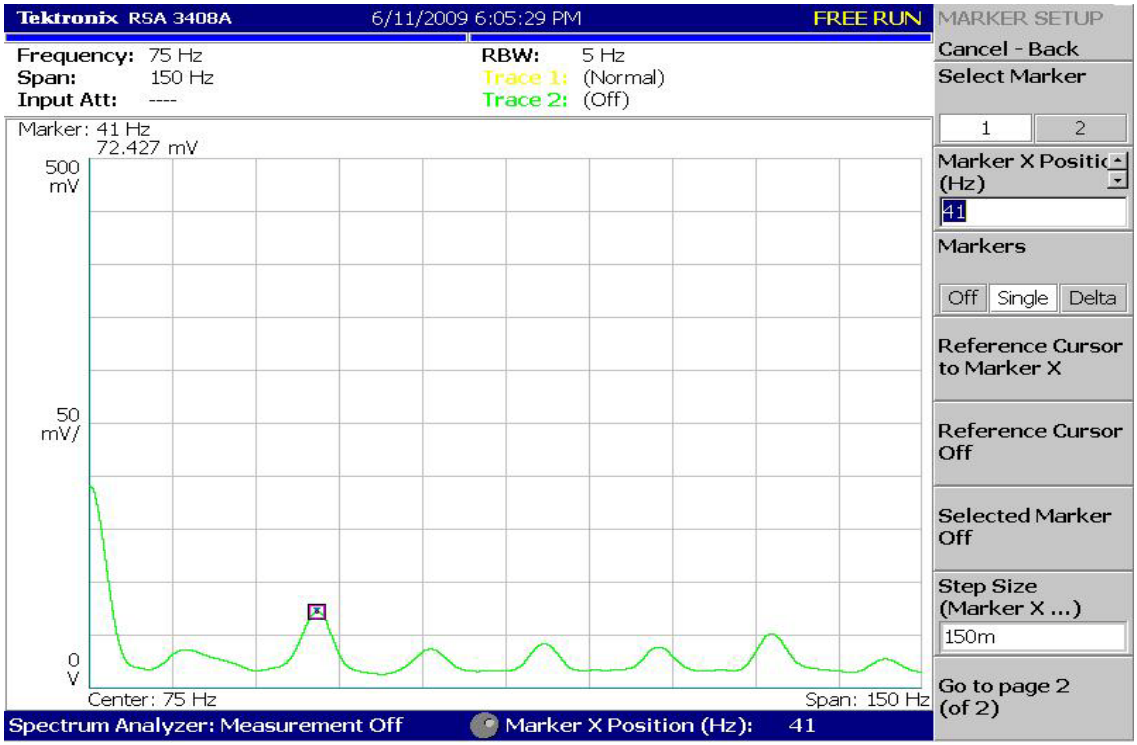

Figure 20. Frequency response for 20 Hz input frequency to the shaker

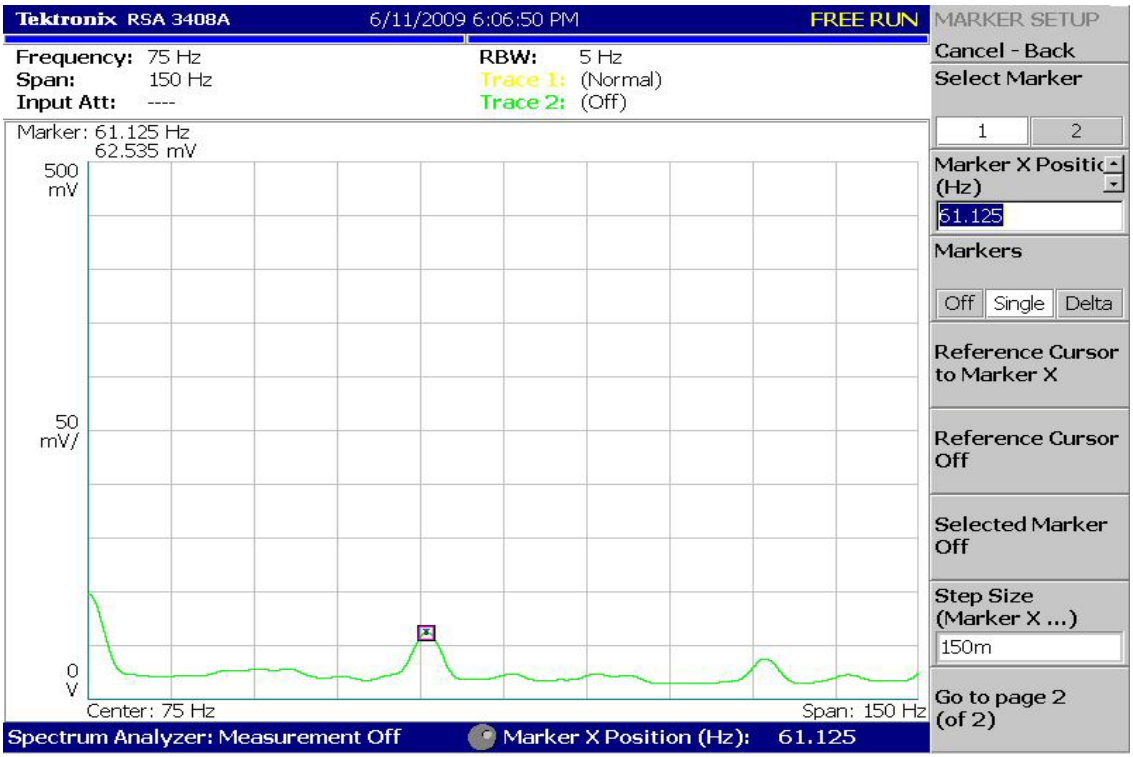

Figure 21. Frequency response for 30 Hz input frequency to the shaker

Figure 22. Frequency response for 40 Hz input frequency to the shaker

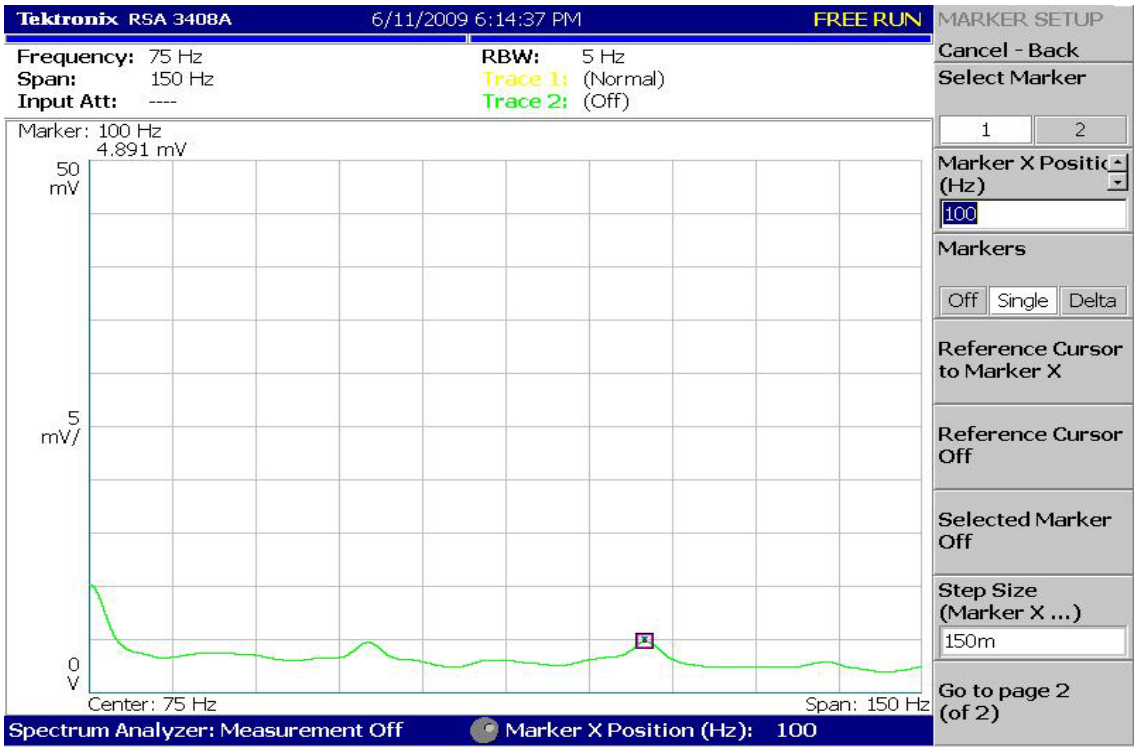

Figure 23. Frequency response for 50 Hz input frequency to the shaker

As observed from the frequency responses above, the peak frequency component occurs at twice the input frequency from the function generator and the other peaks are observed at the harmonics of the input frequency. The output from the switch exhibits some periodicity at the harmonics of the fundamental frequency. Hence, in one cycle of input signal from function generator, the ball bearing manages to make two contacts most of the time. The strength of each frequency component is decreased as the frequency of vibration increases. When the vibration frequency is increased beyond 60 Hz, the ball bearing comes to the stationary position and hence the switch remains in the off state. At the higher frequencies the displacement of the ball bearing is too low to initiate a contact and hence, before the ball bearing makes the contact with the washer, the vibrating device pulls the ball bearing in the reverse direction. When the vibration frequency is decreased below 8 Hz the switch comes to the stationary position, as the strength of

the vibration is very low to produce motion in the ball bearing and the switch remains in off state. This allows us to predict that the maximum and minimum frequency of vibration is dependent on the mass of the ball bearing and the diameter of the washer. As the diameter of the smaller washer is reduced, the peak frequency component shifts to higher frequency. The frequency of contacts made in a single cycle increases with the reduced diameter of the washer because of smaller distance that needs to be traveled by the ball bearing to make successive contacts. This allows us to describe the switching action exhibited by the switch is a function of the diameter of the outer conductor, mass of the ball bearing and the intensity of vibration. Hence, depending upon the environment chosen, the intensity of vibrations will determine the physical dimensions of the washer and the mass of the ball bearing to achieve the desired frequency of switching.

As observed from the experiments, the ball tends to rotate in the shape of n-sided polygons. For a low frequency, the ball makes very few contacts with the washer for one complete rotation of 360 degrees. As the frequency increases, the number of contacts increases and the ball tends to go in circles around the centre as depicted in Figure 24.

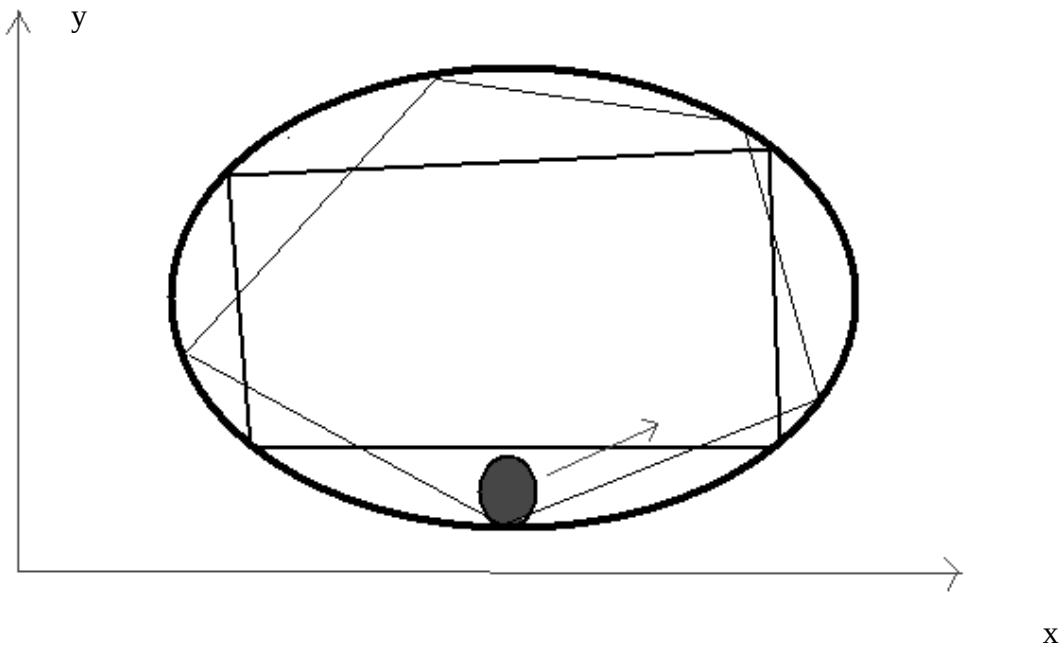

Figure 24. Dynamics of the ball bearing inside the washer

3.3 TUNING THE DESIGN OF SWITCH

From the discussion above, various parameters of the switch can be varied to tune the switch for a particular switching frequency for any given vibration characteristics. Figure 25 illustrates various parameters that can be considered for the design of switch.

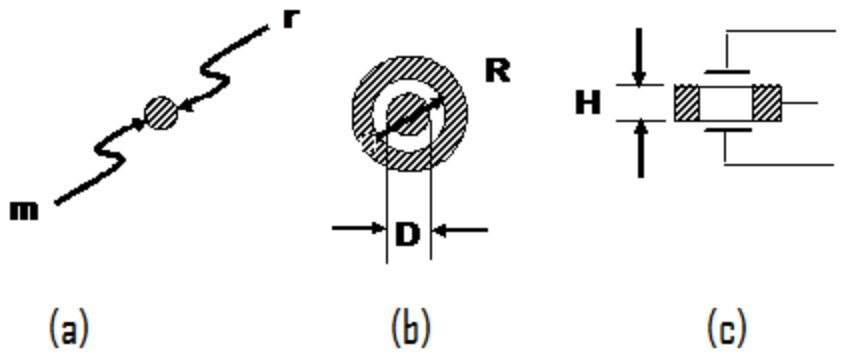

Figure 25. Classification of design parameters of switch

The frequency of the switched output, for a given vibration, is a function of the following parameters:

(1) Radius of the sphere, **r**

(2) Diameter of the Center Conductor, **D**

(3) Height of the Outer Conductor, **H**

(4) Mass of the Spherical Element, **m**

(5) Dimensions of the Outer Conductor, **R**

Given a particular motion, the problem to be solved is described in Figure 26, where a switch is to be designed with the above five (5) parameters to produce the desired frequency for the input motion.

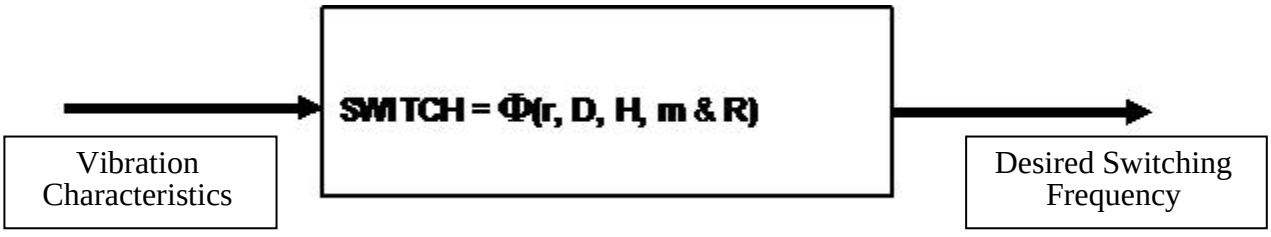

Figure 26. Function block for Tuning the Design of Switch

4.0 DC-DC CONVERSION TECHNIQUES

DC-DC converters are employed in many electronic devices to provide distributed power supplies. They are used in variety of applications like laptop computers, spacecraft power supplies, telecommunication equipment and even in utility power systems applications like high voltage dc transmissions and static VAR compensators. The switching mode converters offer higher efficiency than the traditional linear mode devices. The power levels encountered in high-efficiency switching converters range from less than one watt for low power applications to roughly Megawatts used in utility power systems. For low power applications, the operation is strictly limited by the amount of power available and hence, the need for eliminating the active elements that consume power would be a practical approach to increase the power conversion efficiency. The rest of this thesis work focuses on DC-DC conversion techniques in view of its operation at very low power.

A large number of DC-DC converter topologies are available that can increase or decrease the magnitude of input voltage at the output and/or invert the polarity. Switching converters typically use semiconductor switching devices like MOSFET, BJTs, IGBTs and thyristors. The switching frequency of the devices typically varies from 1 kHz to 1 MHz [6]. The four standard topologies of DC-DC converters are shown in Figure 27.

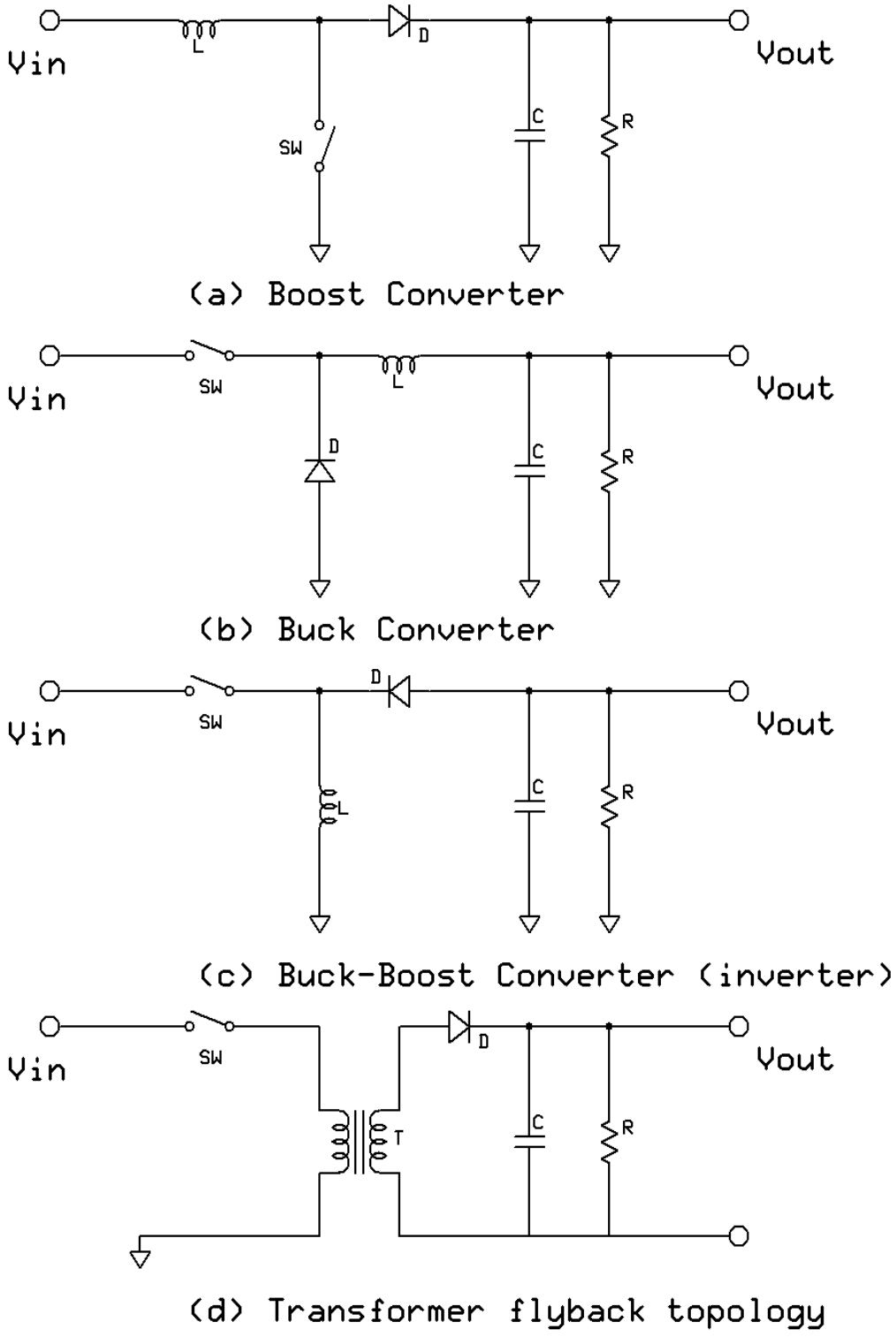

Figure 27. DC-DC converter topologies

Considering the boost converter topology, the conversion factor is obtained by equating the average voltage across the inductor over one switching period to zero [6]. When the switch is in ON state, the voltage across the inductor is equal to the input voltage V_{in}. When the switch is in OFF state, the voltage across the inductor be V_l.

So the output voltage V_{out} is given by:

$$V_{out} = V_{in} + V_l \tag{4.1}$$

The average voltage across the inductor over the switching period is equal to zero.

$$V_{in} * T_{on} = V_l * T_{off} \tag{4.2}$$

$$V_{in} * T_{on} = (V_{out} - V_{in}) * T_{off} \tag{4.3}$$

$$V_{out} = V_{in} * (1 + \frac{T_{on}}{T_{off}}) \tag{4.4}$$

Let D be duty cycle of the switching waveform, the conversion factor is given by

$$\frac{V_{out}}{V_{in}} = \frac{1}{(1-D)} \tag{4.5}$$

where D is given by:

$$D = \frac{T_{on}}{T_{on} + T_{off}} \tag{4.6}$$

Figure 28 shows the plot of conversion ratios of different DC-DC conversion topologies. As observed from the different topologies, the boost converter is used for further study as it outputs higher DC voltage level than the input DC voltage level. Though the Buck-boost, Cuk and SEPIC converters from Figure 28 - (c), (d) and (e) provide a higher magnitude of output voltage, but they run the risk of reducing the output voltage below the input voltage for a very low value of duty cycle.

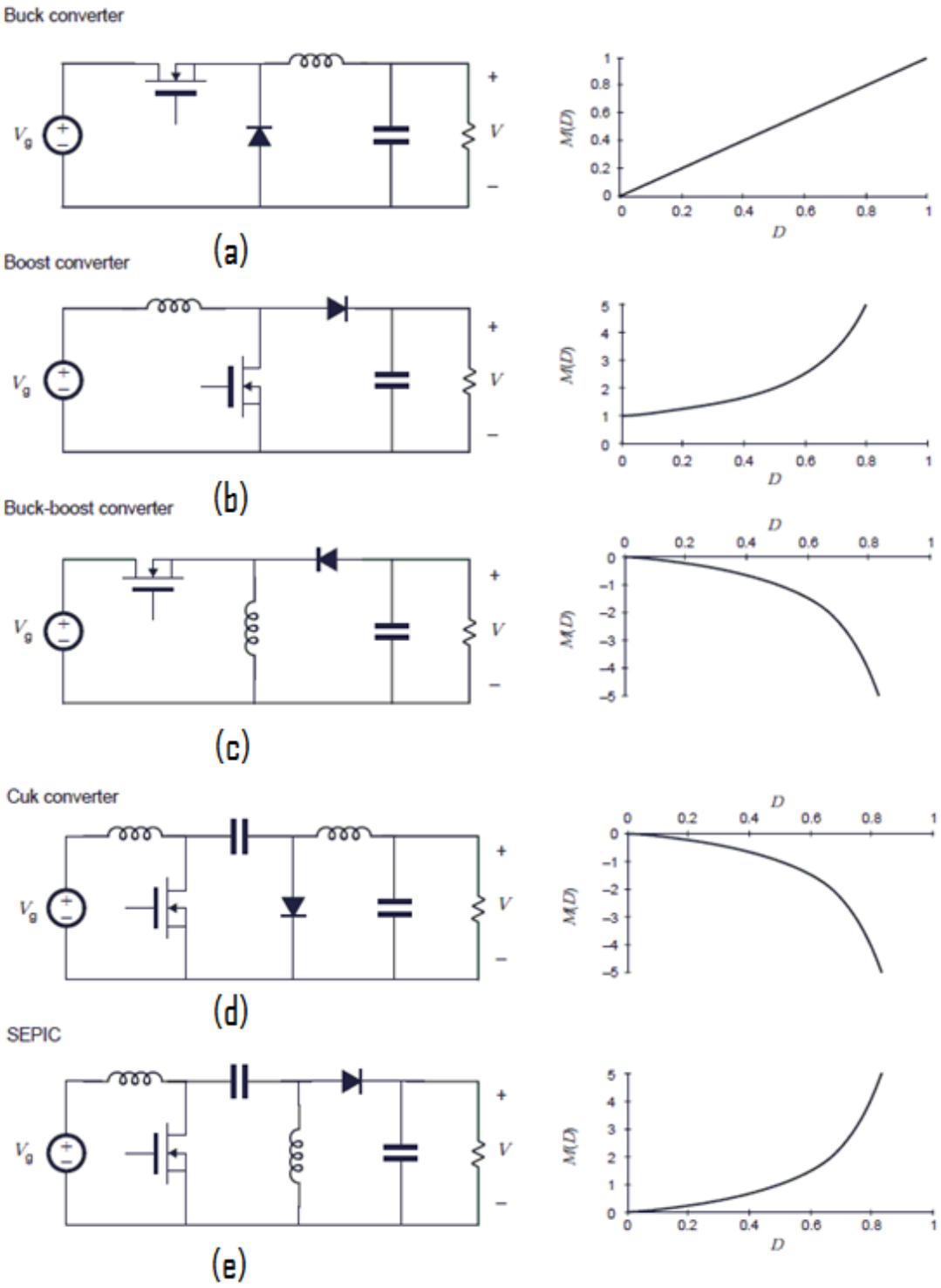

Figure 28. Conversion ratios for different DC-DC converters

Two different circuit topologies are considered for this research namely; (1) boost converter topology and (2) transformer with full wave rectifier topology. The pros and cons of both topologies will be discussed.

4.1 BOOST CONVERTER TOPOLOGY

The voltage and current waveforms of the boost converter are obtained by using the principle of inductor volt-second balance, which states that the average value or DC component of voltage applied across the inductor must be zero [6]. On the converse, we have the charge ampere-second or charge balance principle which states that the average current that flows through the ideal capacitor is zero [6]. Hence, the voltages and currents of DC-DC converters are determined by calculating the average voltage across the inductor and average current across the capacitor and equating them to zero. Though the conversion efficiency of an ideal boost converter is 100%, the conversion efficiency is normally less than 100% due to power dissipation in the inductor resistance and the forward voltage drop of the semiconductor diode. Figure 29 shows the non-ideal boost converter with inductor resistance.

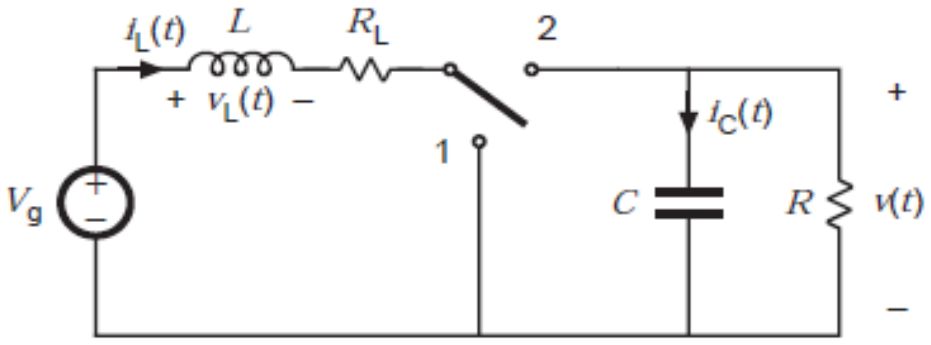

Figure 29. Non ideal boost converter

When the switch is in position 1 in Figure 29, the inductor voltage is given by

$$v_L(t) = V_g - i_L(t)*R_L \quad (4.7)$$

By using small ripple approximation

$$V_L = V_g - I_L R_L \quad (4.8)$$

Likewise the capacitor current can be approximated to

$$I_C = -V/R \quad (4.9)$$

When the switch is in position 2 in Figure 29, the inductor voltage is given by

$$v_L(t) = V_g - i_L(t)R_L - v(t) \approx V_g - I_L R_L - V \quad (4.10)$$

and capacitor current is given by

$$i_C(t) = i_L(t) - v(t)/R \approx I_L - V/R \quad (4.11)$$

Upon equating the average value of $v_L(t)$ to zero we obtain the output voltage

$$0 = D(V_g - I_L R_L) = (1 - D)(V_g - I_L R_L - V) \quad (4.12)$$

Likewise applying the principle of charge balance to capacitor current we have

$$0 = D(-V/R) + (1 - D)(I - V/R) \quad (4.13)$$

From equations (4.12) and (4.13), we have can solve the unknowns V and I_L

$$\frac{V}{V_g} = \frac{1}{(1-D)} \frac{1}{(1+\frac{R_L}{(1-D)^2 R})} \quad (4.14)$$

$$I_L = \frac{V_g}{(1-D)^2 R} \frac{1}{(1+\frac{R_L}{(1-D)^2 R})} \quad (4.15)$$

The voltage conversion ratio M(D) is given by equation 4.14, and it is plotted against the duty cycle of switching waveform (D) for different values of R_L/R. The plot is shown in Figure 30. As observed from the plot, the voltage conversion gain increases with the duty cycle. The

gain increases to a maximum value and rapidly falls to zero for high value of duty cycles. The voltage conversion gain is increased with an increase in load resistance.

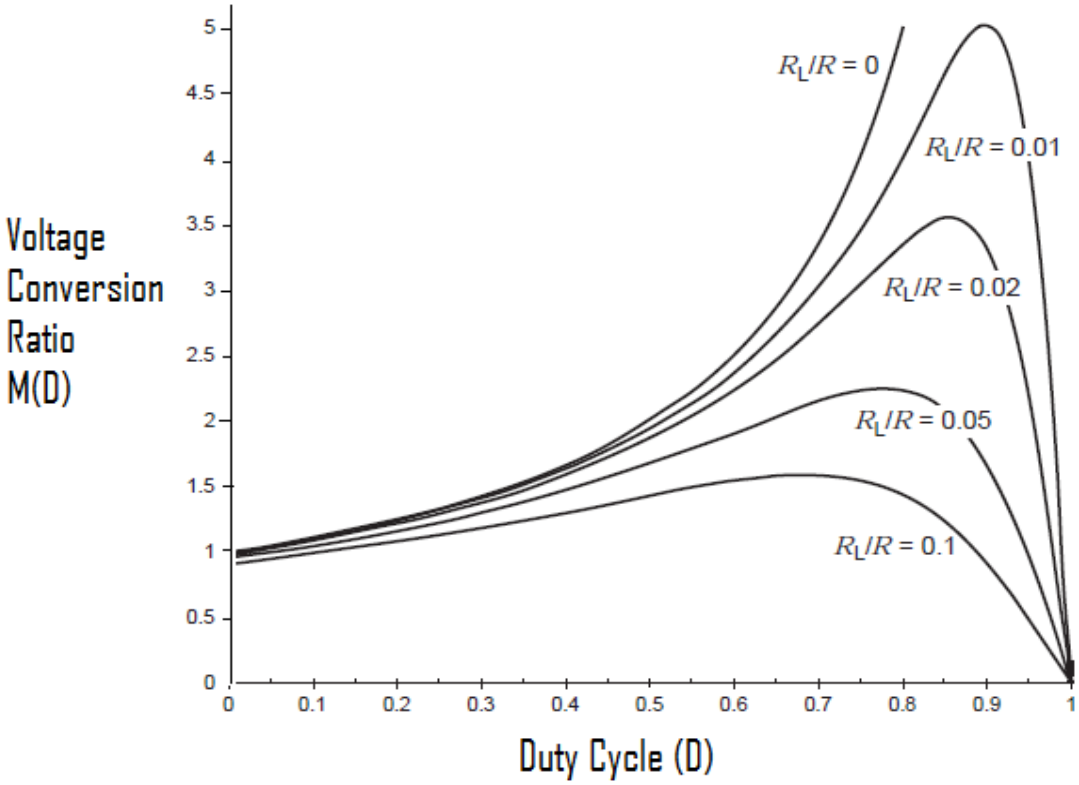

Figure 30. Output voltage vs. duty cycle for non-ideal boost converter

The boost converter efficiency is given by

$$\eta = \frac{P_{out}}{P_{in}} = \frac{(\frac{V^2}{R})}{(V_g I_L)} = \frac{1}{(1+\frac{R_L}{(1-D)^2 R})} \tag{4.16}$$

The efficiency is plotted against the duty cycle for several values of R_L/R in Figure 31. High efficiency is achieved for large values of R as the current flowing through circuit decreases and hence, the power dissipation is reduced. The efficiency also decreases with increase in duty cycle. The efficiency given by equation 4.16 does not include the power delivered to the active

elements as it is considered that the power delivered to active elements is negligible at higher power levels of operation. Hence, this measure would be inappropriate to compare the passive DC/DC conversion technique proposed in this work with existing DC/DC conversion techniques.

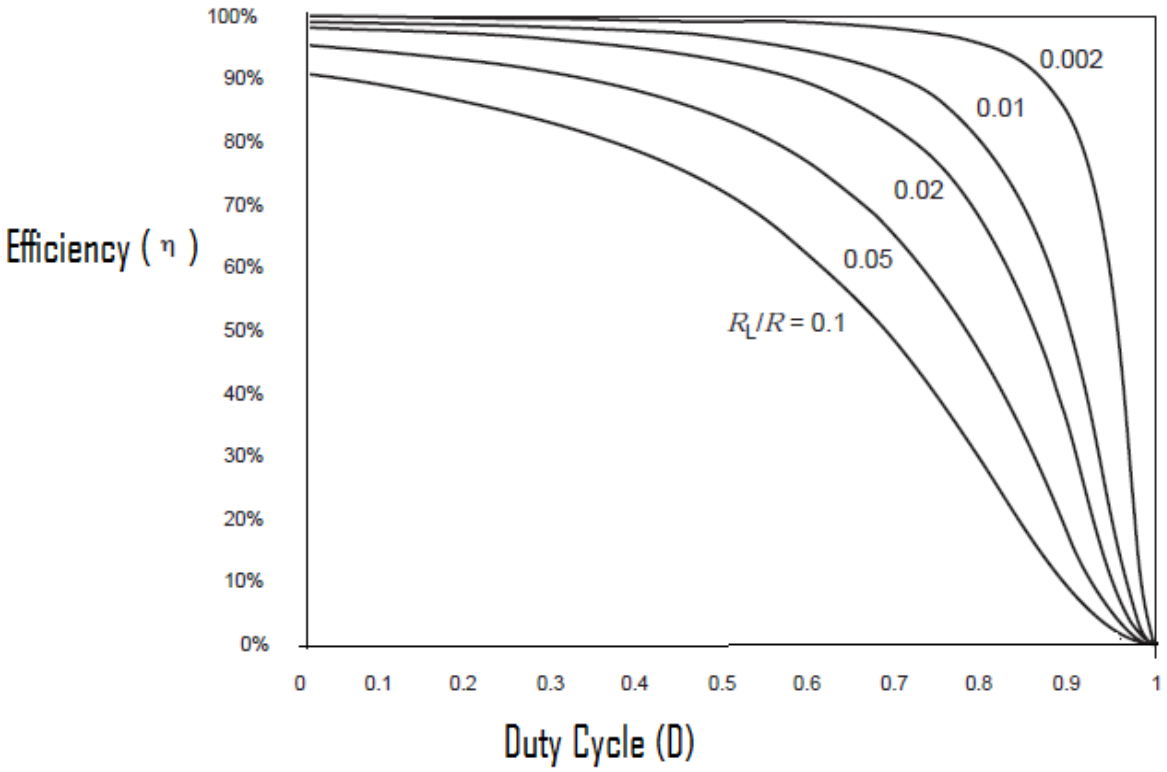

Figure 31. Efficiency vs. Duty cycle for the non ideal boost converter

The output voltage ripple and inductor current ripple can be fixed by choosing appropriate values of inductance and capacitance. The voltage and current ripples are given by the equations below [6].

$$\Delta i_L = \frac{V_g}{2L} DT_s \tag{4.17}$$

$$\Delta v = \frac{V}{2RC} DT_s \tag{4.18}$$

The high frequency components and its harmonics present in the DC voltage can be further reduced by choosing suitable inductor and capacitor combinations and thereby, reducing the ripple in the output DC voltage. The series LC circuit of the boost converter acts as a low pass filter with the corner frequency given by [6]

$$f_0 = \frac{(1-D)}{\sqrt{LC}} \tag{4.19}$$

The low pass LC filter will further eliminate the high frequency components without any loss of power.

4.2 TRANSFORMER TOPOLOGIES

The transformer can be used in DC-DC converters to obtain isolation between the input and the output. Whenever a high ratio of step down or step up conversion is required, the transformer can provide an optimized solution by choosing appropriate value of turn ratio (n). The size of the transformers can be limiting factor for application in low power applications, and this thesis work makes an attempt at reducing the size of transformers by using printed PCB transformers.

4.2.1 Transformer Flyback Topology

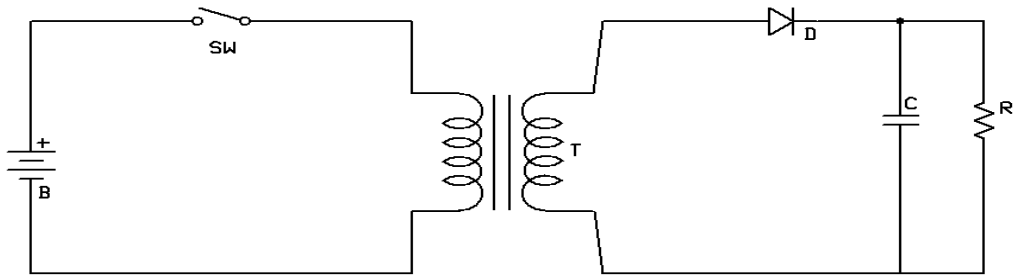

Figure 32. Transformer flyback topology

The transformer flyback converter is similar to operation of the buck-boost converter shown in Figure 32. The current doesn't flow simultaneously between the primary and the secondary windings of the transformer. The magnetizing current is switched between the primary and the secondary windings. For the transformer flyback topology is shown in Figure 32, when the switch 'SW' is in closed state, current flows through the primary inductor of the transformer, and the diode is reverse biased and no current flows through the secondary winding. Energy is stored in the magnetic field of the flyback transformer. When the switch SW is in open state, the magnetic field induces current in the secondary coil which forward biases the diode. Energy stored in magnetic field is transferred to the DC load. The current conversion ratio of the transformer flyback converter is given by:

$$M(D) = n * \frac{D}{(1-D)} \tag{4.20}$$

Where n is the transformer turns ratio and D is the duty cycle of switching waveform. But the transformer flyback converter runs the risk of generating output voltages less than the input voltage for low values of duty cycle.

4.2.2 Transformer with Full Wave Rectifier Topology

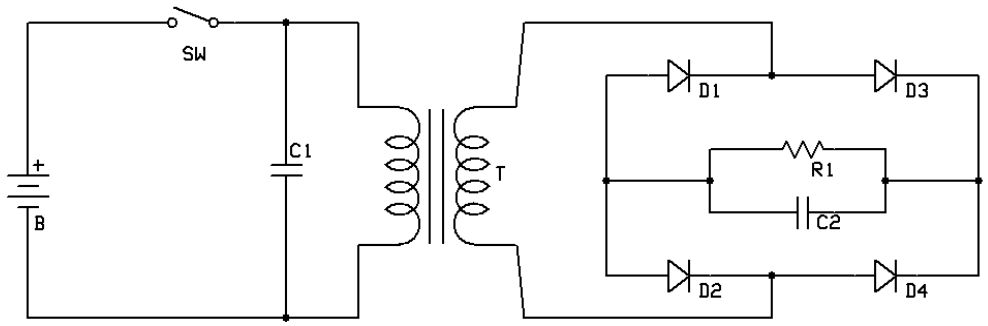

Figure 33. Transformer topology with full wave rectifier

The DC-DC conversion circuit shown in Figure 33 consists of a switch, a transformer and a full wave rectifier. The principle of this method is to convert the DC signal to AC signal using the switch. The AC signal is then applied to the transformer primary windings which induce voltage across the secondary windings. Unlike the flyback converter, the current flows simultaneously in both the windings. The output from the secondary windings is full wave rectified, and a capacitor placed across the output terminals outputs the DC voltage by reducing the ripple in the rectified signal.

The size of the transformer is a concern in achieving higher power densities. In aiming to reduce the size of the transformer, printed coreless PCB transformers are created [7]. The printed PCB transformers are shown in Figure 34 and Figure 35.

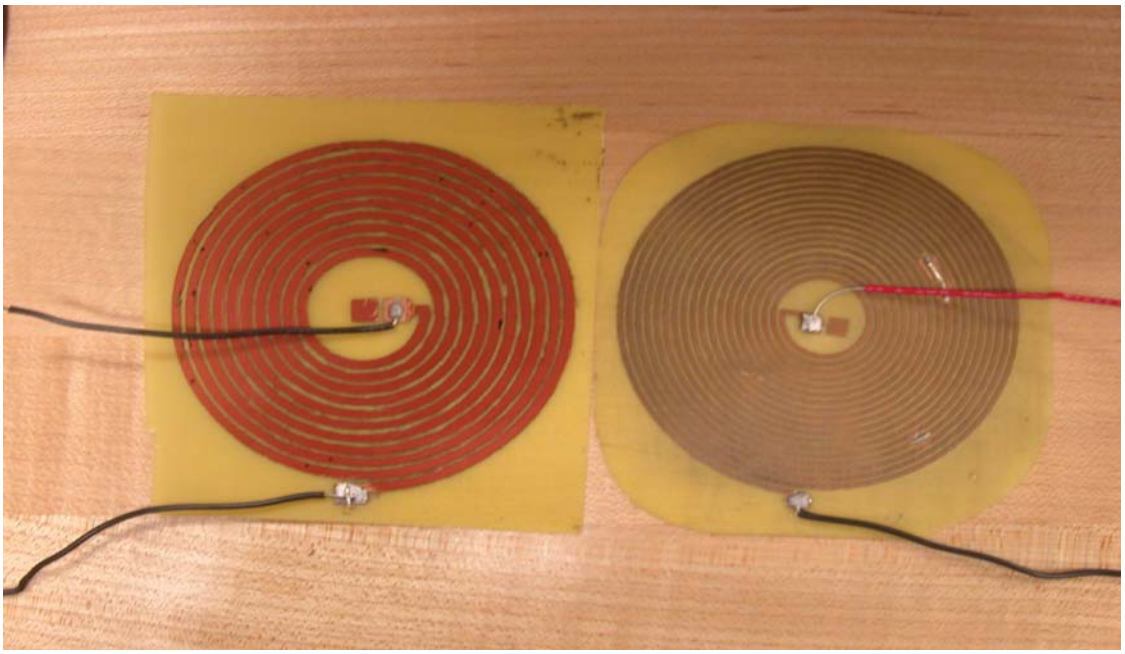

Figure 34. PCB printed transformers- Primary coil (left) and Secondary coil (right)

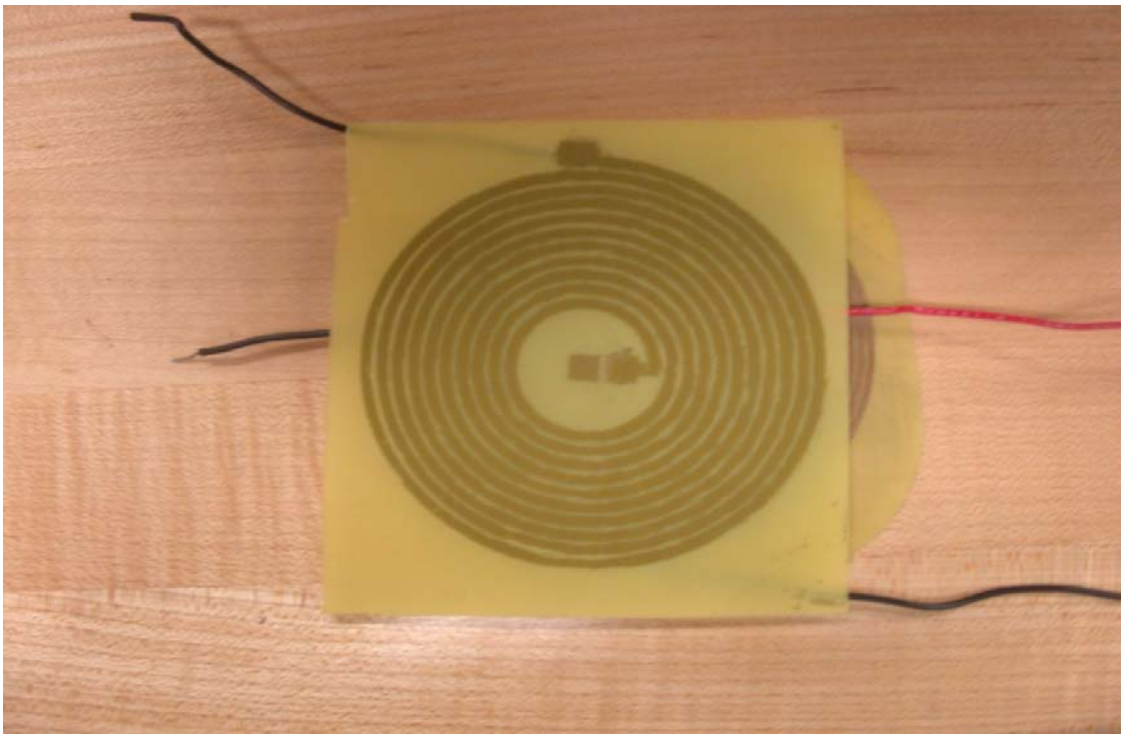

Figure 35. PCB printed transformers- Coils placed one over the other

The primary coil of the printed PCB transformers shown in Figure 34 and Figure 35 has 9 turns and the secondary coil has 18 turns. The inductance of the primary coil (Lp) is 3.9 uH and inductance of the secondary coil (L_s) is 10.6 uH.

4.3 MOTION ACTIVATED SWITCH IMPLEMENTATION

Boost converter topology is now considered for further study and the active transistor switch is replaced with the passive electro-mechanical switch. The switch is subjected to vibrations using the electro-dynamic shaker. DC voltage from the DC power supply is provided to the circuit. The voltage gain obtained from the boost converter is compared with the transformer topology with a full-wave rectifier.

4.3.1 Boost converter implementation

The schematic of boost converter circuit is shown in Figure 36, where the switch SW is replaced with the previously discussed electro-mechanical switch. The values of the inductance (L1) and capacitance (C1) are chosen as 27uH and 10uF. The input voltage from the DC supply (Vin) is 3 volts. The frequency of vibration of the shaker is varied from 10 Hz to 40 Hz and the output across the load resistor R1 is measured. The load resistance is varied from 10 kOhm to 500 kOhm. Figure 37 shows the graph for the output voltage against load resistance (R1) for different values of vibration frequencies.

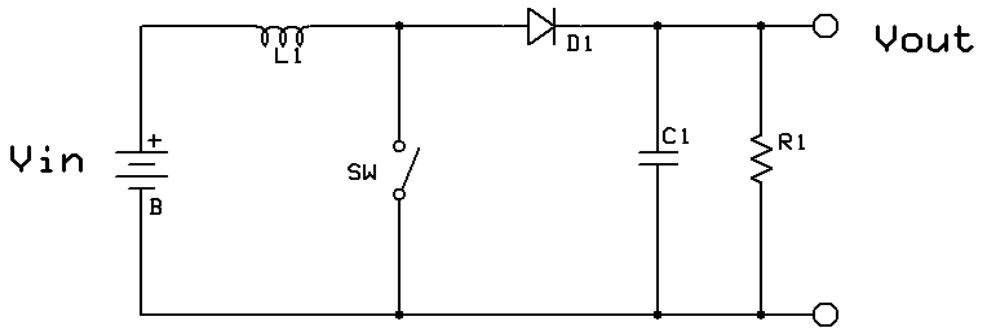

Figure 36. Schematic of boost converter

Table 2. Output voltage measured across varying load for different vibration frequencies

Resistance (R1)- kOhms	Voltage (Vout) – volts			
	Frequency = 10Hz	Frequency = 20Hz	Frequency = 30Hz	Frequency = 40Hz
10	5 v	3 v	2.7 v	2.7 v
50	10 v	4 v	2.7 v	2.7 v
100	15 v	6 v	3 v	2.7 v
200	22 v	10 v	3 v	2.7 v
500	32 v	20 v	4 v	2.7 v

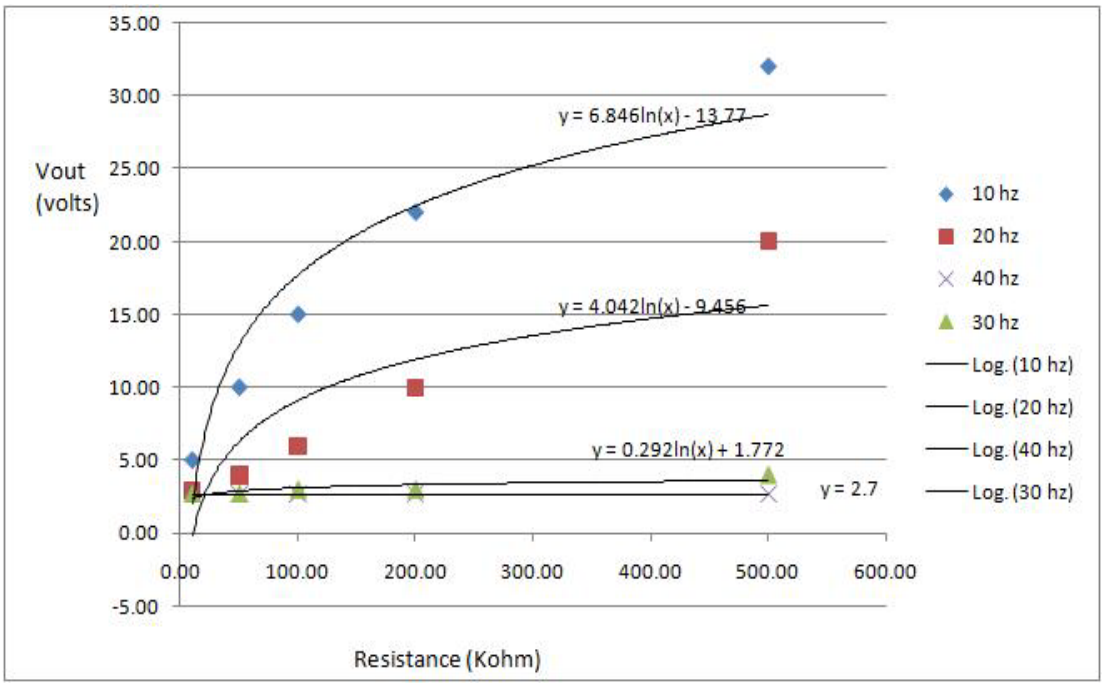

Figure 37. Output voltage vs. load resistance for different vibration frequencies

As the frequency of vibration increases, the gain of the boost converter decreases. At a frequency of 40 Hz and beyond, the output voltage is almost constant. The output voltage is less than the input voltage due to the voltage drop across the diode.

By choosing appropriate values of inductance, load resistance and the capacitance values with L1 = 27 uH, R1 = 200 kOhm and C1 = 10 uF, the input voltage DC voltage is varied from 1 volt to 4 volts and readings are plotted for different vibration frequencies. Figure 38 shows the graph of the output voltage plotted against the varying input for different vibration frequencies.

Table 3. Output voltage measured for varying input voltage for different frequencies

Input Voltage (Vin) - volts	Output Voltage (Vout) - volts		
	Frequency = 10 Hz	Frequency = 20 Hz	Frequency = 30 Hz
1.00 V	3.5 V	2.7 V	1.50 V
2.00 V	11.0 V	6.0 V	2.3 V
3.0 V	21.0 V	10.0 V	2.6 V
4.0 V	32.0 V	22.0 V	3.6 V

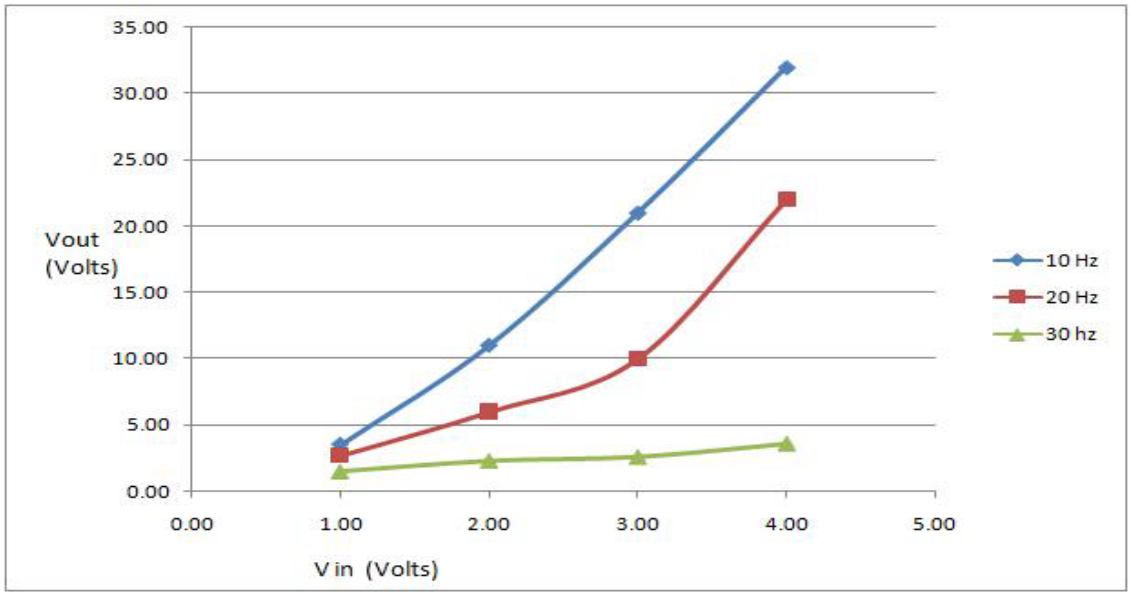

Figure 38. Output voltage vs. input voltage for different vibration frequencies

The output voltage increases linearly with the increase in input voltage. With an increase in frequency, the output falls below the input voltage. Hence, depending upon the physical properties of the switch, the switch tunes to a specific vibration frequency where the boost

converter circuit exhibits the highest conversion ratio. For the electro-mechanical switch, at 10 Hz vibration frequency, the boost converter circuit achieves a higher conversion factor.

4.3.2 Transformer topology with full wave rectifier implementation

The switch SW in Figure 33 is replaced with the passive motion activated switch and the transformer chosen is a ferrite core transformer with turn ratio 1:100. The switch is excited by vibrations at 10 Hz frequency from the function generator and 3 volts of input DC signal is applied to the primary circuit of the transformer. The value of the capacitor across the primary winding C1 = 1 nF, resistor R1 = 10 kOhm and capacitance C2 = 22 uF. Figure 39 and Figure 40 indicate the voltages at the primary and secondary windings of the transformer.

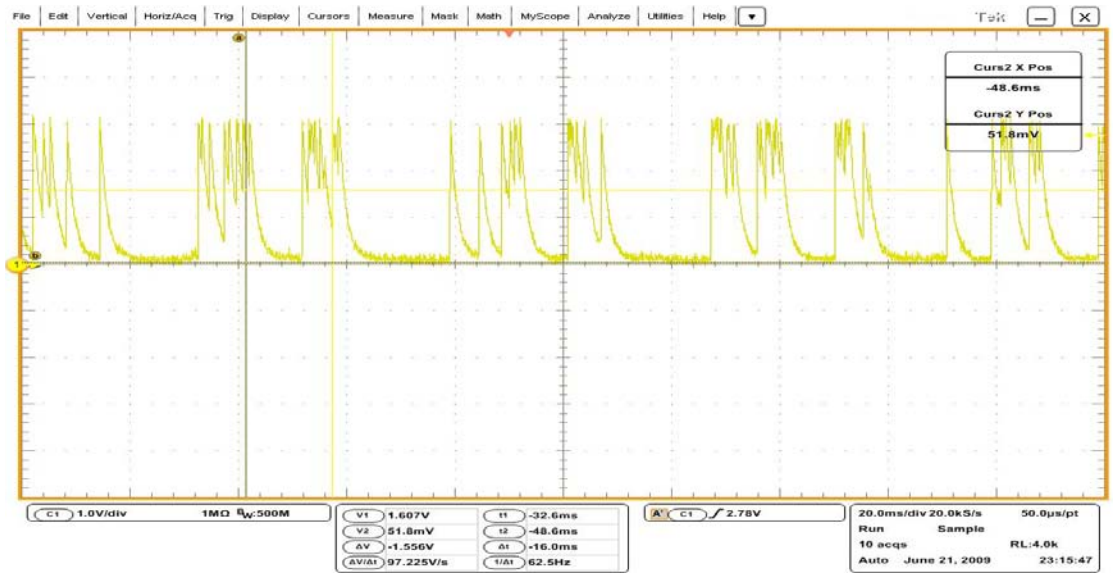

Figure 39. Voltage at the primary winding of the transformer

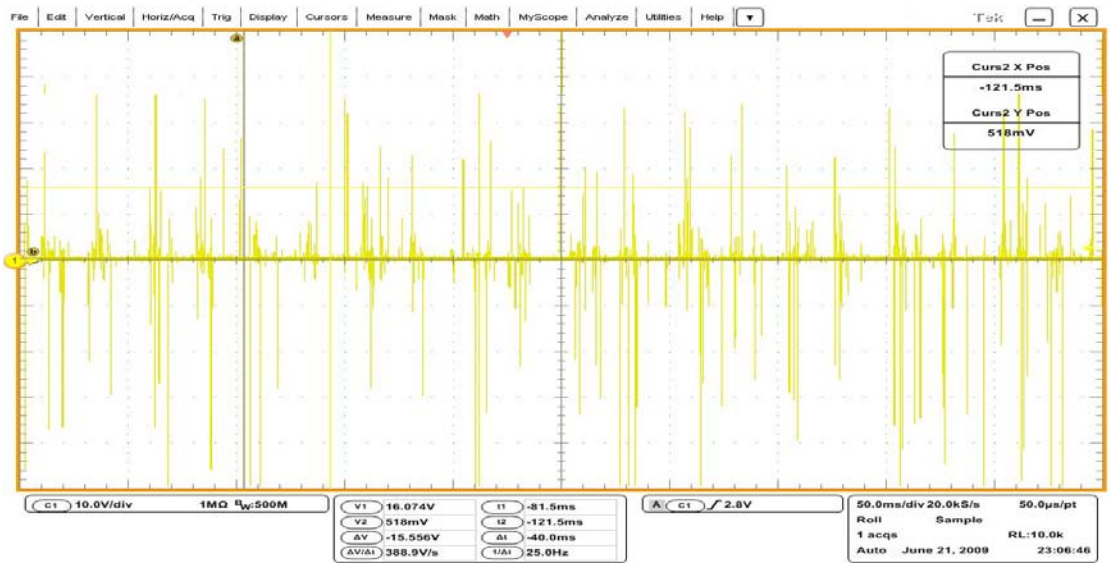

Figure 40. Voltage at the secondary winding of the transformer

The DC voltage obtained after rectification is 20 volts across the load resistance R1 with a negligible amount of ripple. When the input frequency is increased beyond 30 hz, the voltage induced on the secondary coil decreases. Figure 41 illustrates the voltage at the secondary coil for input vibration frequency of 40 Hz from the function generator.

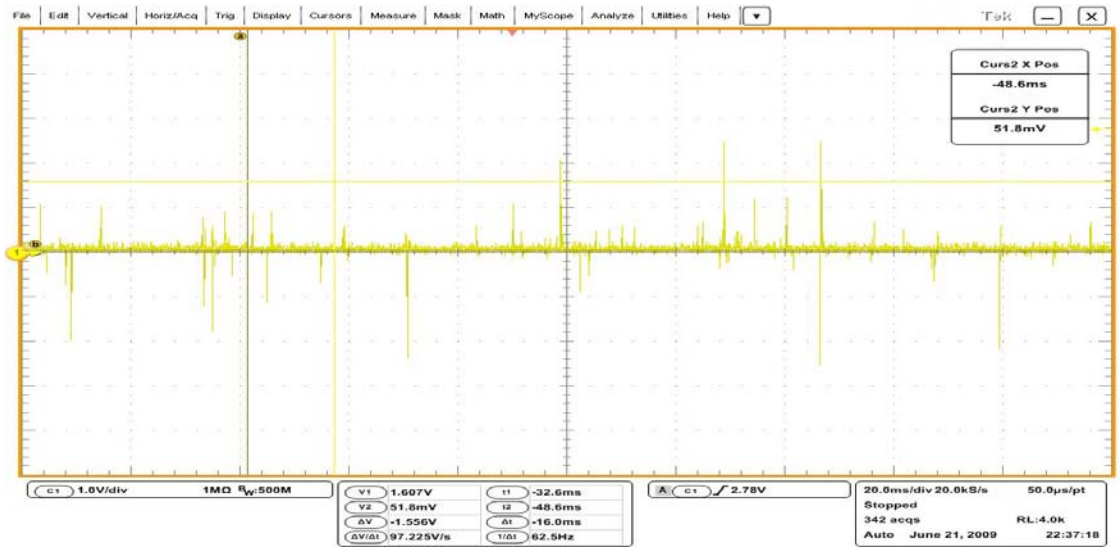

Figure 41. Voltage at the secondary winding of the transformer

The DC voltage obtained at the output after rectification is less than one volt with large ripple factor. Further increase in vibration frequency from the function generator will lead to zero output voltage across the load and thereby completely zeroing the power available at the output though there is sufficient power available at the input terminals. This would be a limiting factor when the vibrations in environment are not consistent and can lead to drop in the power available to rest of the circuit.

The air core printed PCB transformer is used by placing the primary and secondary coils one over the other in lieu of ferrite core transformer. The output voltage induced at the secondary windings is analyzed with the input DC voltage fixed at 3 volts, and the value of resistor and capacitances are the same as those used in Figure 36 (C1 = 1nF, R1 = 10 kOhm and C2 = 22 uF). The switch is subjected to vibration frequency of 10 Hz from the function generator. Figure 42 indicates the voltage induced on the secondary coil of the printed PCB transformer.

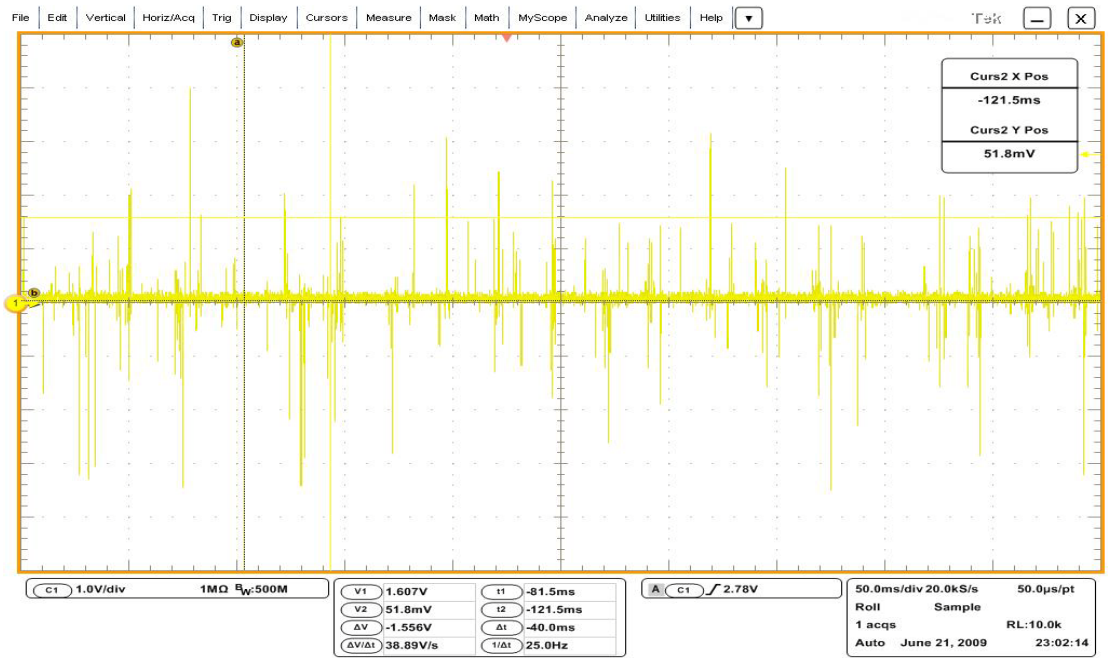

Figure 42. Voltage at the secondary winding of the printed PCB transformer

The DC voltage across the load resistance after rectification is 2.4 volts which is less than the input voltage 3 volts. Proper design of the printed PCB transformer would achieve high voltage and also reduce the size of the transformer. Multiple printed PCB transformers can be placed in series to achieve high voltage gains. This experiment above demonstrates that higher power densities can be achieved using the printed PCB transformers.

5.0 APPLICATION IN RFID SYSTEMS

The DC-DC conversion technique can be applied to RFID devices to boost the DC voltage to higher voltages required by the data processing unit when there is sufficient power available at the input terminals. The RFID devices operate on low power constraints where power is supplied by on-board batteries or from the energy harvested by the device from the reader's transmission. Passive tags draw the power required for their operation from the electromagnetic field transmitted by the reader. The RF energy radiated by the reader induces RF voltage in the passive tag's antenna which is rectified by an N-stage charge pump to provide DC voltage supply for the transponder. The power available to the tag is used by the digital section to perform data processing and to transmit back the modulated signal to the reader. Hence, the operating range of the tag is strictly dependent upon the power available. To maximize the operating range, the power-matching network must be tuned to allow maximum power transfer and the RF to DC conversion circuit should be highly efficient to reduce the conversion losses. The problem becomes much more challenging at very low levels of power consumption around 1 μWatt. Though, most of the previous work focuses on the tuning the receiving circuit to allow maximum power transfer [8][9] , this thesis focuses on implementing the DC-DC conversion techniques to output higher voltage levels at very low power levels. By employing the passive DC-DC conversion technique, high voltage levels are achieved at very low conversion losses.

5.1 IMPLEMENTATION OF DC-DC CONVERSION TECHNIQUE

The passive DC-DC conversion circuit implementing the boost converter topology is used for step-up conversion of DC voltage generated after the rectification of the radio frequency signal – the initial DC input. Figure 44 shows the block diagram description for implementing the passive DC-DC conversion technique. Figure 44-(a) indicates the implementation using an antenna and matching circuit. The impedance matching of the antenna with the rest of the circuit would be very challenging due to the non-linear nature of the circuit elements. Initially, the matching can be done by an annealing approach given in [9], where different combinations of tuning circuit elements are implemented until high voltages are recorded. As the focus of the thesis is improving the output voltage levels after rectification of RF signal from the antenna, in lieu of antenna and the matching circuit, a signal generator is substituted to input the RF signal to the rectification circuitry. Figure 44-(b) indicates the implementation using the signal generator. The RF signal at 125 kHz is applied to the rectification circuitry. The voltage doubler circuit uses a HSMS-280x series Schottky diode as shown in the Figure 43.

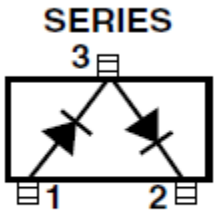

Figure 43. Series Schottky diode

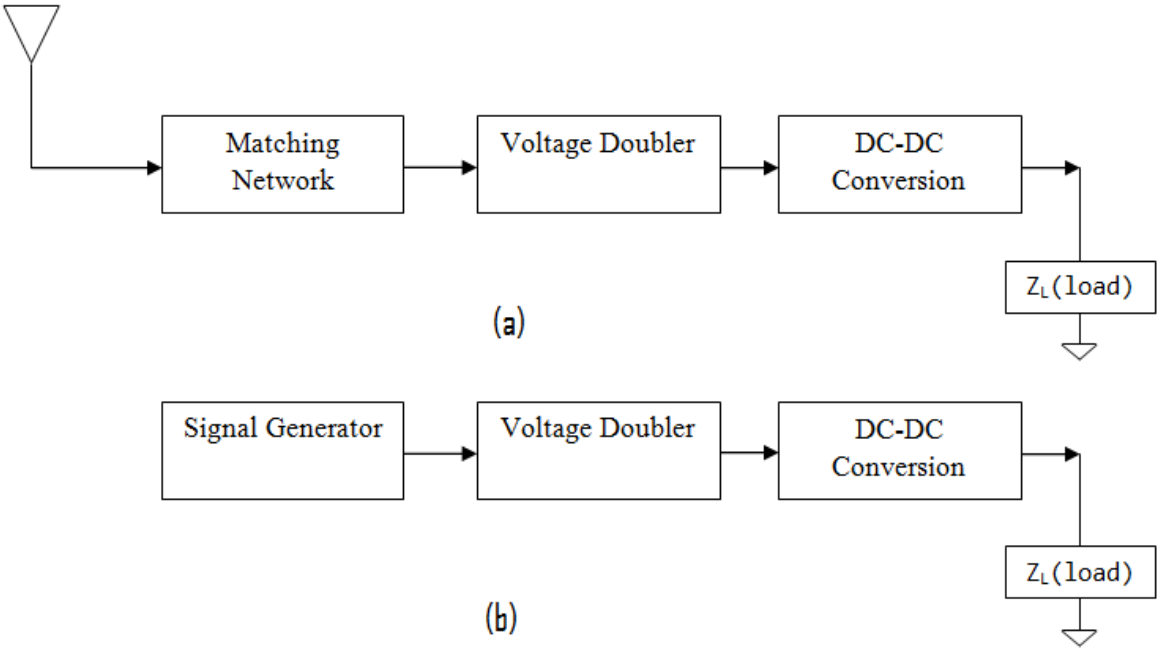

Figure 44. DC-DC conversion technique Implementation in RFID devices

(a) Antenna with matching network (b) Vector Signal generator

The antenna followed by the matching network shown in Figure 44-(a) is replaced by a vector signal generator (Rohdes & Schwarz) as shown in Figure 44-(b). Using the signal generator would allow varying the power of the signal and also the frequency of the transmitted signal. Figure 45 shows the schematic of the circuit implementing the DC-DC conversion technique where the input RF signal is fed from the signal generator and the value of the load resistance (R1) is varied to observe the voltage conversion ratio for different loads.

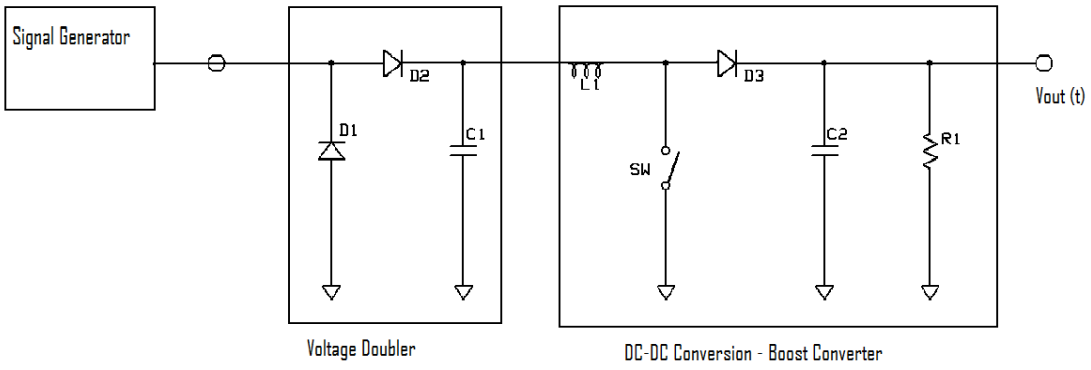

Figure 45. DC-DC Conversion implementation - Schematic

The RF signal of 125 kHz frequency is applied to the circuit at 18 dBm power level. The DC voltage obtained after rectification is 3 Volts. The values of the circuit elements chosen are capacitance C1= 10 uF, C2 = 20 uF and inductor L1 = 22 uH. The diode D3 is a schottky diode with 0.4 Volts forward voltage drop. The output voltage is measured across the resistance R1. The voltage observed for different values of R1 are listed in Table 4.

Table 4. Output Voltage for different resistance values

Serial No	Power Level	DC voltage after rectification	Load Resistance (R1)	Output Voltage (Vout(t))
1	18 dBm	3 Volts	13.6 K	3 Volts
2	18 dBm	3 Volts	27.2 K	3.2 Volts
3	18 dBm	3 Volts	75 K	4.4 Volts
4	18 dBm	3 Volts	155 K	5.1 Volts

As the frequency of the radio frequency signal increases beyond 10 MHz, the voltage observed at the output terminals is very low due to losses in the circuitry as the circuit elements are not optimized for high frequency operations. As a result, sufficient input voltages were not generated across the resistor. The circuit must be optimized for high frequency radio signal to reduce the losses. From results in Table 4, higher voltages are realized by employing the proposed DC/DC conversion technique.

6.0 CONCLUSION AND FUTURE WORK

In this work, a new technique for DC-DC conversion is proposed which utilizes the passive motion-activated electro-mechanical switch by replacing the active transistor element. The functionality of the proposed technique is proved by implementing the motion activated switches in different DC-DC conversion topologies. The pros and cons of different configurations are verified. The switching characteristics of the switch for different intensities of vibrations are studied which would assist in tuning the design of switch based on the vibration characteristics of the environment. In view of reducing the size of the onboard components and to achieve high power densities, printed PCB transformers are used for the study to prove the feasibility of replacing the ferrite core transformers. The benefit of the proposed technique in low-power applications is demonstrated by implementing the technique in RFID devices which operate on low power constraints. The DC-DC conversion can be used to generate higher voltages required by the data processing circuitry at the same power levels, and at the same time reducing the power conversion losses by eliminating the power consuming transistor elements.

Miniaturization of the proposed technique by implementing micro-switches would be a topic of interest for low power applications where many micro-switches can be placed in parallel and/or series configurations to achieve efficient switching phenomena. Hence, the active elements in the circuit can be replaced by the passive switching elements for the environments which can induce constant motion in each of the individual switching elements. As the

practicality of the approach has been proven, the future work should focus on implementing a on-chip passive DC-DC conversion technique to generate higher voltages for data processing logic. Hence, realizing efficient data processing systems even at lower power levels (<1μWatt).

6.1 CONTRIBUTION OF THE RESEARCH

- ✓ The ability to amplify low DC input voltage to a sufficient voltage capable of switching transistors, using the passive motion-activated switch has been researched and demonstrated.
- ✓ The properties of motion-activated switch to harvest the vibration energy have been classified and the parameters of the switch to tune the design of switch to perform efficiently at a given intensity of vibration have been discussed.
- ✓ Different traditional DC-DC conversion topologies have been studied and the boost-converter has been chosen over other topologies to develop a custom DC-DC conversion circuit.
- ✓ From the research above, a working proto-type system has been developed capable of DC amplification.
- ✓ Sufficient time has been spent in determining the effectiveness of using air core printed PCB transformers to obtain the necessary AC amplification.
- ✓ Practical application of the research in the field of RFID has been demonstrated.

BIBLIOGRAPHY

[1] Michael T. Zhang, Milan M. Jovanovic and Fred C. Lee, “Design consideration for low-voltage on-board DC/DC modules for next generations of data processing circuits", *IEEE Trans. on Power electronics*, Vol. II, No. 2,1996.

[2] Giuseppe De Vita and Giuseppe Iannaccone, “Design criteria for the RF section of UHF and microwave passive RFID transponders”, *IEEE trans. on microwave theory and techniques*, Vol. 53, No. 9, 2005.

[3] K. Finkenzeller, “RFID handbook, radio-frequency identification fundamentals and applications,” *John Wiley & Sons*, Chichester, 1999.

[4] C.A. Balanis, “Antenna Theory: Analysis and Design”, *John Wiley & Sons*. 1997.

[5] Motion activated electrical switch, US patent No. 7,315,004 B1, Dawar technologies, Pittsburgh, PA, Peter W. Jarzynka and H. Gene Baumgarten, Filed August 24, 2006(29 claims).

[6] Robert W. Erickson, Dragan Maksimovic. “Fundamentals of Power Electronics”, *by Springer*. (2006).

[7] S.C. Tang, S.Y. Hui and Henry Shu-Hung Chung,”Coreless Planar Printed-Circuit-Board (PCB) Transformers – A fundamental concept for signal and energy transfer”, *IEEE Trans. on power electronics*, Vol. 15, No. 5, 2000.

[8] K.V. Seshagiri Rao, Pavel V. Nikitin and Sander F. Lam, “Antenna design for UHF RFID tags: A review and a practical application”, *IEEE trans. on antennas and propagation*, Vol. 53, No. 12, 2005.

[9] Minhong Mi, Marlin H. Mickle, Chris Capelli and Harold Swift, “RF energy harvesting with multiple antennas in the same space”, *IEEE antennas and propagation magazine*, Vol. 47, No. 5, 2005.